UMTRI-2011-10

PMHS Impact Response in Low and High-Speed Nearside Impacts

University of Michigan
Transportation Research Institute

Carl S. Miller
Jonathan D. Rupp

June 2011

UMTRI-2011-10

PMHS Impact Response in Low and High-Speed Nearside Impacts

University of Michigan Transportation Research Institute

Carl S. Miller
Jonathan D. Rupp

The University of Michigan
Transportation Research Institute
Ann Arbor, MI 48109-2150
U.S.A.

June 2011

Technical Report Documentation Page

1. Report No.	2. Government Accession No.	3. Recipient's Catalog No.
UMTRI-2011-10		

4. Title and Subtitle	5. Report Date
PMHS Impact Response in Low and High-Speed Nearside Impacts	June 2011
	6. Performing Organization Code XXXXXX
7. Author(s) Miller, C.S. and Rupp, J.D.	8. Performing Organization Report No. UMTRI-2011-10
9. Performing Organization Name and Address **The University of Michigan** **Transportation Research Institute** **2901 Baxter Road** **Ann Arbor, Michigan 48109-2150 U.S.A.**	10. Work Unit no. (TRAIS) 11. Contract or Grant No. DTNH22-05-H-01020
12. Sponsoring Agency Name and Address NHTSA, Human Injury Research Division	13. Type of Report and Period Covered 14. Sponsoring Agency Code

15. Supplementary Notes

16. Abstract

Lateral impact tests were performed using seven male post-mortem human subjects (whole, unembalmed cadavers) to further characterize the response of the body, and in particular the force-deflection response of the lower abdomen, to lateral impact. All tests were performed using a dual-sled, side-impact test facility. A multi-segmented impactor was mounted on a sled that was pneumatically accelerated into a second, initially stationary sled on which a cadaver subject was seated facing perpendicular to the direction of impact. Sizes and heights of impactor segments were adjusted for each subject so that forces applied to different anatomic regions including thorax, abdomen, greater trochanter, iliac wing, and thigh could be independently measured on each cadaver. For all tests, the impactor contact surfaces were located in the same vertical plane except that the abdomen plate was offset 5.1 cm toward the subject. Each subject was first impacted on one side of the body using an initial impactor speed of 3 m/s. Following the five of these tests that did not result in injury, the contralateral side of the body was impacted at a speed of either 8 m/s or 10 m/s. The masses of the sleds and the force-deflection characteristics of the energy-absorbing material that acted as the interface between the sleds were set so that the velocity history of the impactor sled matched the average driver door velocity history produced in a series of side NCAP tests. Impactor padding was also selected so that average ATD pelvis and thorax responses from the same series of side NCAP tests were reproduced when the ATD used in these tests was impacted using the average door-velocity history.

Results of these tests were used to develop force-deflection response targets for the abdomen, force history response targets for the pelvis (iliac wing and greater trochanter), the midthigh, and the thorax at each of the three impact velocities. Response targets for the lateral acceleration of the pelvis were also developed. Future work will compare side impact ATD responses to these response targets.

17. Key Words	18. Distribution Statement
side impact, response, abdomen, pelvis	Unlimited

19. Security Classification (of this report)	20. Security Classification (of this page)	21. No. of Pages	22. Price
None	None	48	

CONTENTS

LIST OF FIGURES

LIST OF TABLES

ACKNOWLEDGEMENTS

This research was funded by the National Highway Traffic Safety Administration under contract number DTNH22-10-H-00288. The authors are grateful to Brain Eby and Charles Bradley for the production of test fixtures, to Nathaniel Madura for the development of data processing routines and the design of test fixtures, and to Tom Jeffreys for the assistance in specimen preparation. The authors are also grateful to Rodney Rudd and Steve Ridella for their advice on all phases of this project.

INTRODUCTION

The responses of the human pelvis, abdomen, and thorax to lateral impact have been extensively studied in tests in which post mortem human subjects (whole, unembalmed cadavers) were impacted with ballistic pendulums, decelerated into instrumented impact walls, and dropped onto impactors. Useful data have been collected from each type of test; however, each type of test has important limitations.

Studies in which the mid thorax and lower thorax/upper abdomen have been impacted with flat-faced pendulums have provided the most widely cited data on the force-deflection responses and injury tolerances of these body regions (Eppinger et al. 1978, Viano 1989, Pintar et al. 1997, Shaw et al. 2006, Kemper et al. 2008). However, pendulum impacts do not recreate the simultaneous loading of multiple body regions that occurs when a vehicle occupant interacts with the door in real-world nearside impacts. As a result of this, pendulum impacts produce different subject kinematics and greater rates of body mass recruitment than occur in side impacts. For these reasons, force histories and force-deflection responses at higher levels of deflection measured in previous pendulum impact tests do not reflect the responses that likely occur in moderate to severe real-world crashes, although low-deflection responses may be representative of the initial responses when focal door intrusion initially loads a particular body region before contact with other body regions occurs.

The most common type of whole-body side impact test has been a Heidelberg-style sled test in which a post-mortem human subject (PMHS) seated facing sideways on a low-friction surface slides in to a sled-mounted impact wall (Kallieris et al. 1981, Kallieris et al. 1994, Cavanaugh et al. 1990a and 1990b**,** Pintar et al. 1997, Maltese et al. 2002, Hallman et al. 2010). The velocity at which the cadaver contacts the wall is typically the deltaV of the sled pulse. The impact wall is segmented and instrumented with load cells so that forces applied to different body regions can be independently measured. The horizontal offsets of segments of the impact wall toward the body are varied to preferentially load body regions in a manner that simulates loading due to door intrusion.

Force histories and force-deflection data from Heidelberg-style tests have been used to define the response characteristics of the WorldSID thorax, pelvis, and shoulder (Cesari et al. 2001). However, Heidelberg-style pure lateral impact tests have a number of important limitations including that:

(1) The deceleration pulses used in these tests are equivalent to the cadaver contacting a stationary wall at a constant velocity, which differs from the real-world loading scenario where a nearside occupant is contacted by an intruding door at a velocity that rapidly decreases as the door intrudes.
(2) No tests conducted to date have scaled the sizes or adjusted the heights of impactor segments to account for variations in subject size. As a result, portions of the impactor designed to load particular body regions for one cadaver size loaded parts of adjacent body regions for smaller or larger cadavers.

(3) The large distance that the cadaver must slide prior to contact with the impact wall makes it difficult to control cadaver posture at impact and to repeatably load specific anatomic regions between tests.
(4) Measurements are confounded by differences in body shape between subjects that can change the timing of impactor contact with different body regions and thereby change load sharing between body regions and occupant kinematics.

In addition to Heidelberg-style tests, the side-impact responses of the pelvis, thorax, and abdomen have been measured by dropping whole cadavers onto rigid and deformable rectangular impactors offset toward either the pelvis, lower abdomen, or mid thorax (Walfich 1980, Bendjellal et al. 1984). The forces measured in these tests have been used as targets for subsequent side-imact dummy development, but the abdomen and thorax deflections measured in these tests have not been used, as they were determined from analysis of film, which has been judged to be less reliable than current deflection measurement techniques using chestbands or high-speed VICON systems (Rouhana 2002, Kuppa et al. 2003, Shaw et al. 2010, Lessley et al. 2010). Further, the abdomen responses measured in these tests may be unreliable because the test methods produce unrealistic organ positions at the time of abdomen contact.

Recent side-impact tests have addressed some of the limitations of previous tests. Lessely et al. (2010) overcame the difficulties in controlling cadaver position and posture present in Heidelberg-style side-impact tests by impacting an initially stationary cadaver at a constant velocity with a moving wall and by using a custom-designed system that independently controlled position and posture. Yoganandan et al. (2011) adjusted the horizontal offsets of impact wall segments so that all segments contacted their target body regions at the same time.

Nevertheless, as a result of the methodological limitations of previous test series discussed above, several important aspects of human lateral impact response have not been well documented. In particular, only Heidelberg-style sled tests conducted by MCW have measured lower abdomen deflection using chestbands (Pintar et al. 1997, Maltese et al. 2002, Yoganandan et al. 2007, Hallaman et al. 2010). However, only three of these tests used an abdomen offset, and the abdomen response data measured in tests using flat walls, or pelvic and thorax offsets, are confounded by differences in subject shapes and by test methods that did not scale impactor size with subject size.

Most whole-body, side-impact sled tests in which deflection has been measured using techniques that are accepted as reasonably accurate have used impact speeds of 6.7 m/s and 8.9 m/s (Pintar et al.1997, Maltese et al. 2002, Petitjean et al. 2009). However, real-world crash data and three 4.3 m/s PMHS impacts performed by Lessley et al. (2010), which are the only “low-speed” nearside PMHS impact data collected to date, demonstrate that serious thorax injuries can occur in low-severity lateral impacts. In addition, previous pure lateral impact sled tests used constant velocity pulses, while, as indicated above, in many real-world lateral impact crashes, door velocity decreases as the door intrudes toward the occupant as a result of the acceleration of the struck vehicle and deceleration of the striking vehicle.

The current study was performed with three goals. These were to (1) provide additional data on the response of the lower abdomen to lateral impact, such as occurs when nearside occupants are loaded by an intruding door in a real-world side impact crash, (2) provide additional data on the response of the body to low-speed lateral impact using loading conditions that reproduce the decrease in door velocity that occurs with increasing door intrusion in side impact, and (3) characterize the responses of different anatomic body regions in a manner that is unaffected by subject size. To achieve these goals, seven whole cadavers were impacted using a custom-designed, sled-to-sled side-impact test facility, where a sled on which a segmented impactor is mounted impacts a second, initially stationary sled on which an occupant is seated. This configuration generates impactor velocity histories that mimic the decrease in door velocity that occurs with increasing door intrusion in SNCAP MDB crash tests.

METHODS

A series of lateral impacts was performed using seven cadavers to estimate the impact response of the human male cadaver abdomen as well as the responses of the iliac wing, greater trochanter, and mid-thigh. Table 1 describes these cadavers and the twelve tests in which these cadavers were used. All cadavers were male and were obtained from the University of Michigan Anatomical Donations Program. Prior to testing, cadavers were screened for pre-existing fractures or skeletal abnormalities that could affect impact response using a head-to-toe computed topography (CT) scan performed using a 1.25 mm slice size. Specimens were stored frozen and thawed to room temperature prior to testing.

Each subject was exposed to a low-severity lateral impact with an initial impactor velocity of 3 m/s. This speed was intended to measure sub-injury response. Following this impact, each subject was CT scanned a second time to determine if any skeletal injuries were produced. In five of seven 3-m/s impacts, no or minimal skeletal injuries were observed, so a higher severity test with an initial impactor velocity of either 8 m/s or 10 m/s was performed on the previously untested side of the subject (see Table 1). In subsequent sections of this paper, Test Series IDs appended with an "A" represent initial low-severity impact (e.g., NBA0901A). Test IDs appended with a "B" represent the subsequent high-severity impact.

Table 1. Description of Test Specimens

Test Series ID	Age	Gender	Stature (cm)	Mass (kg)	t-score*	Tests Performed		
						3 m/s	8 m/s	10 m/s
NBA0901	86	M	170	77	-1.8	X		X
NBA0902	61	M	185	82	-0.9	X		
NBA0903	50	M	173	64	1.6	X		X
NBA1004	66	M	173	79	-	X	X	
NBA1005	51	M	183	98	2.6	X	X	
NBA1006	34	M	188	102	2.0	X	X	
NBA1107	87	M	175	73	-	X		

* t-scores obtained using the Osteogram method (Yang et al. 1994).

Test Facility

Tests were performed using a custom-designed, dual-sled test facility illustrated in Figure 1. This facility consists of a 725-kg "impact" sled on which a segmented, padded impact wall is attached and a second 360-kg "occupant" sled on which the specimen is seated. Force-deflection characteristics of the padding and the procedure used for assessing these padding force-deflection characteristics are contained in Appendix A. Tests were performed by pneumatically accelerating the impact sled to the desired initial loading velocity. After reaching this velocity, the impact sled contacted the occupant sled as the load wall contacted the cadaver. After loading of the test specimen was complete and the impact and occupant sleds decoupled, both sleds were stopped at a deceleration rate of 1 g to 2 g using a series of pneumatic brakes. A thickly padded catch (not shown in Figure 1)

attached to the far side of the occupant sled was used to control the subject motion after impact and to prevent post-event injuries.

Figure 2 illustrates the impact wall and the occupant sled. The impact wall was segmented to allow independent loading of the subject's thorax, abdomen, iliac wing, greater trochanter, and mid thigh. The shoulder was not loaded in this study because of concerns that small variations in shoulder position could have large effects on whole-body kinematics and load-sharing between body regions.

Segments of the impact wall were adjustable so that they could be aligned with the target anatomical regions for different sized subjects. Sizes of the plates in impact wall were varied for each cadaver to ensure that each plate always loaded the same anatomic region. In particular, the size and position of the thorax plate was scaled so that the top of the plate was immediately below the axilla of a raised arm (about the 4^{th} rib laterally) and so that the bottom of the plate was at the top of the 9^{th} rib laterally. The plate that loaded the abdomen was scaled so that the top was at the level of the 10^{th} rib and the bottom was just above the superior margin of the iliac wing. Sizes and positions of the plates that loaded the greater trochanter and iliac wing were not scaled, as the baseline sizes for these plates were such that they loaded the target body regions for all subjects. For all tests, the section of the impact wall aligned with the abdomen was offset 5.1 cm toward the subject relative to the other loading plates.

Forces applied to each plate in the impact wall were independently measured by one or two triaxial load cells attached to each plate. Measured forces were inertially compensated using accelerometers attached to each plate.

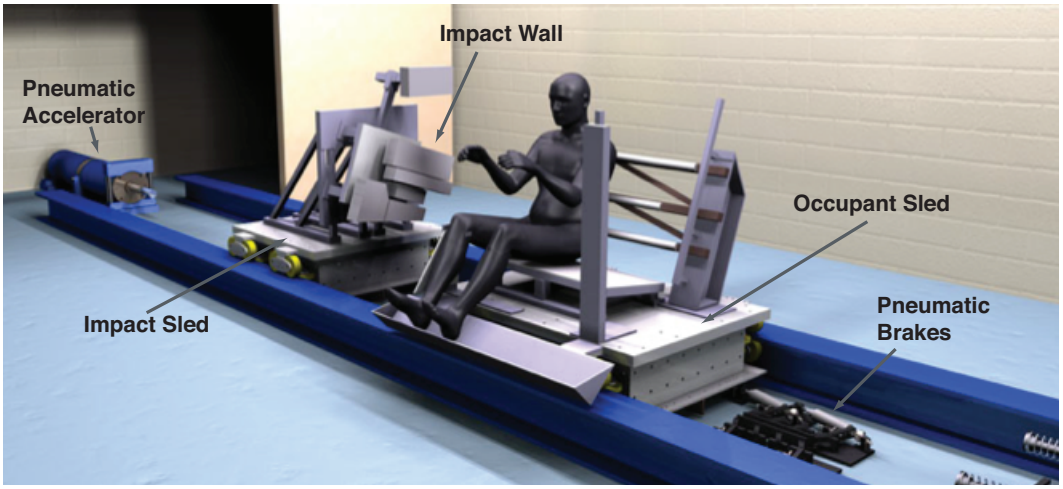

Figure 1. Rendering of UMTRI's dual-sled impact facility.

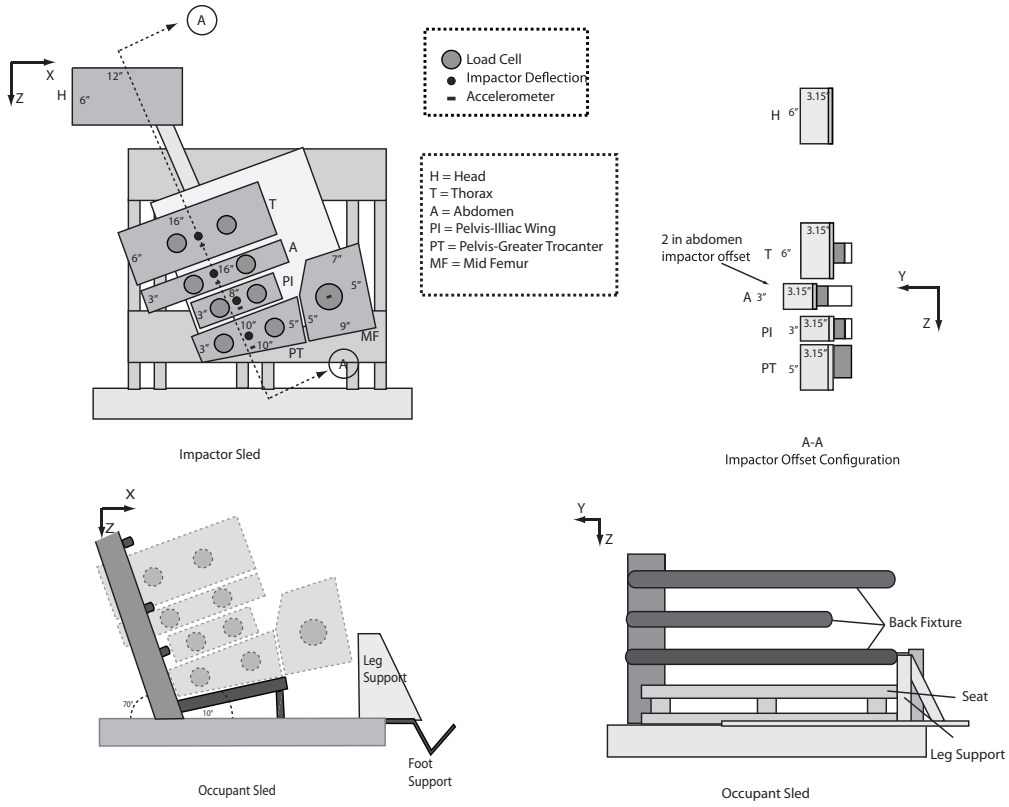

Figure 2. Illustrations of the segmented impact wall and the occupant sled.

Impactor Velocity Profiles

Low-severity tests were performed with an initial 3-m/s loading velocity of the impactor wall. High-severity tests were performed using an initial impact velocity of either 10 m/s or 8 m/s. Impactor velocity histories for the 10 m/s and 8 m/s tests were selected to fall within mean±1 SD response corridors for door velocity histories determined from analyses of SNCAP tests conducted between 1999 and 2005 in which door accelerations were measured (Klinich et al. 2008). Comparisons between these corridors and impactor velocity histories used in the 3-m/s, 8-m/s, and 10-m/s tests are shown in Figure 3. Energy absorbing material (Hexcel) placed between the sleds was used to control the deceleration of the impacting sled and the acceleration of the occupant sled in all tests. For the 10-m/s tests, the size and crush strength of this energy absorbing material were selected so that the decrease in impact sled velocity following sled-to-sled contact was similar to the average decrease in door velocity in the SNCAP tests. The size and crush strength of energy absorbing material used in the 10-m/s tests were maintained for the 8 m/s tests, although the velocity of the impactor sled was decreased so that velocity of the loading wall at the time of occupant contact was approximately 1 SD below the mean of the SNCAP tests. For both 8-m/s and 10-m/s tests, the impactor wall contacted the subject at the same time that the impactor sled contacted the occupant sled. In the 3-m/s tests, the impactor contacted the subject before the impact sled contacted the occupant sled so that loading of the occupant was complete before sled-to-sled contact.

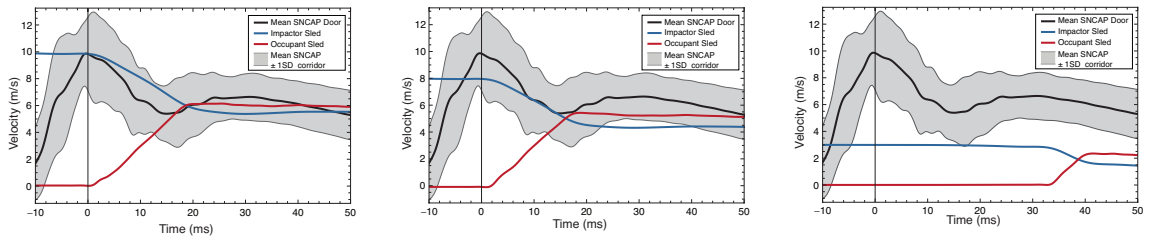

Figure 3. Comparison of impactor and occupant sled velocities to mean ±1 SD SNCAP mid-door velocity corridors for the 10 m/s (left), 8 m/s (center), and 3 m/s (right) dual-sled test conditions.

To prevent focal loading of the thorax and to provide a more realistic loading condition, each section of the impact wall was covered with 80-mm thick sections of Microcell 1900 foam (72 kPa). This particular type and thickness of foam was selected to produce SID HIII pelvis and lower-spine accelerations in the 10-m/s test condition that were similar to those measured in SNCAP tests from which the door velocity corridors were derived, as shown in Figure 4.

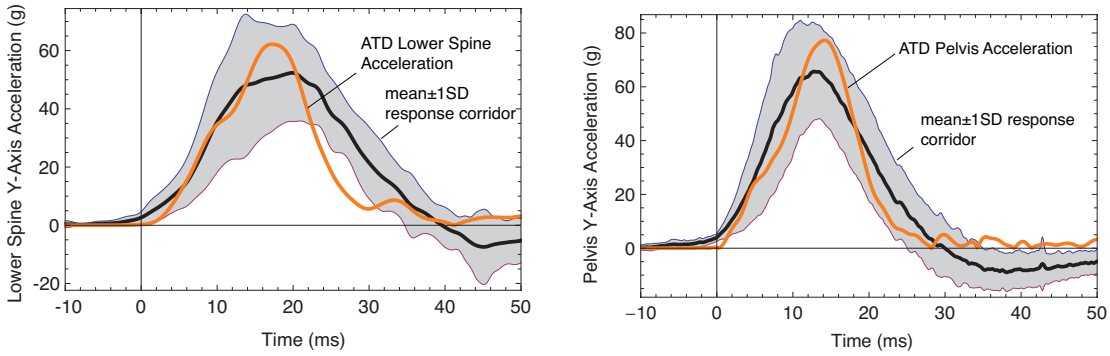

Figure 4. Comparison of SID HIII lower spine (left) and pelvis (right) acceleration histories produced from 10-m/s pilot tests to ± 1 SD response targets developed from SNCAP data.

Specimen Instrumentation and Preparation

Figure 5 illustrates the locations of all thoracic instrumentation attached to the test specimens. Chestbands were positioned around each specimen at the mid-thorax and abdomen. For all tests, a 59-channel chestband was used to measure abdomen contour. A 59-channel chestband was used to measure thorax contour in tests NBA0903 through NBA1007. The ends of the chestbands were overlapped and fixed such that the circumference of the band remained constant during loading. The chestbands were attached to their corresponding spinal accelerometer mounts to provide fixed spine reference points. Each specimen was also instrumented with three orthogonal accelerometers and three orthogonal angular rate sensors attached to T1, to the mid-thoracic spine on the vertebral body that was at the same height as the area between the 4th and 5th ribs laterally (T7 or T8), and to the vertebral body in the lumbar spine that was at the same height as the area immediately below the 10th rib, laterally (L3). A three-axis

accelerometer block was also attached to the sacrum and accelerometers were attached to the most lateral aspects of ribs 4, 6, 8, and 10 on the struck side, and ribs 6 and 10 on the non-struck side. Strain gages were attached to struck-side ribs 5 through 10 to record fracture timing. After all instrumentation was attached, the specimen was dressed in a tight-fitting black leotard and the subject's facial features were obscured by a section of stockinet.

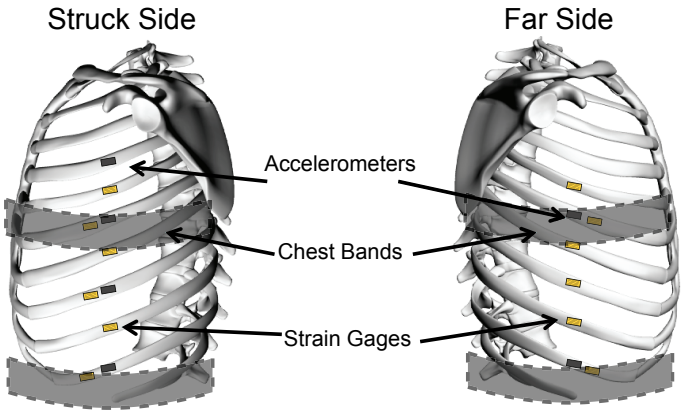

Figure 5. Locations of the chestbands, rib accelerometers, and strain gages relative to the ribs and spine.

Subject Positioning

Figure 6 shows a pre-test image of the subject posture and position used in all tests. Each subject was seated on a rigid seat that was designed with seat and seat back angles that allowed the torso and lower extremities to be positioned in an automotive-seated posture. The seat back consisted of three horizontal supports that were designed to allow the motion of the specimen's spine to be observed and to prevent interference with spinal accelerometers and chestband mounts. The surfaces of the support that contacted the subject's back were covered with lengths of Teflon with a dome-shaped cross-section. As shown in Figure 6, these back supports were positioned so that the top support was between the T1 accelerometer block and the thorax chestband, the middle support was between the thorax chestband and the L3 accelerometer block, and the lower support was between the abdomen chestband and the sacrum accelerometer block. The seat was covered with a thin sheet of Teflon. The postures of the upper extremities and head were controlled with strings attached to these regions and to the superstructure located above the subject. Each string was attached to a thin piece of cloth tape that was partially torn immediately prior to testing so that any motion of the subject would cause the tape to tear and allow the subject to move without constraint. Thus, the approach to controlling subject posture prior to impact has no effect on impact response.

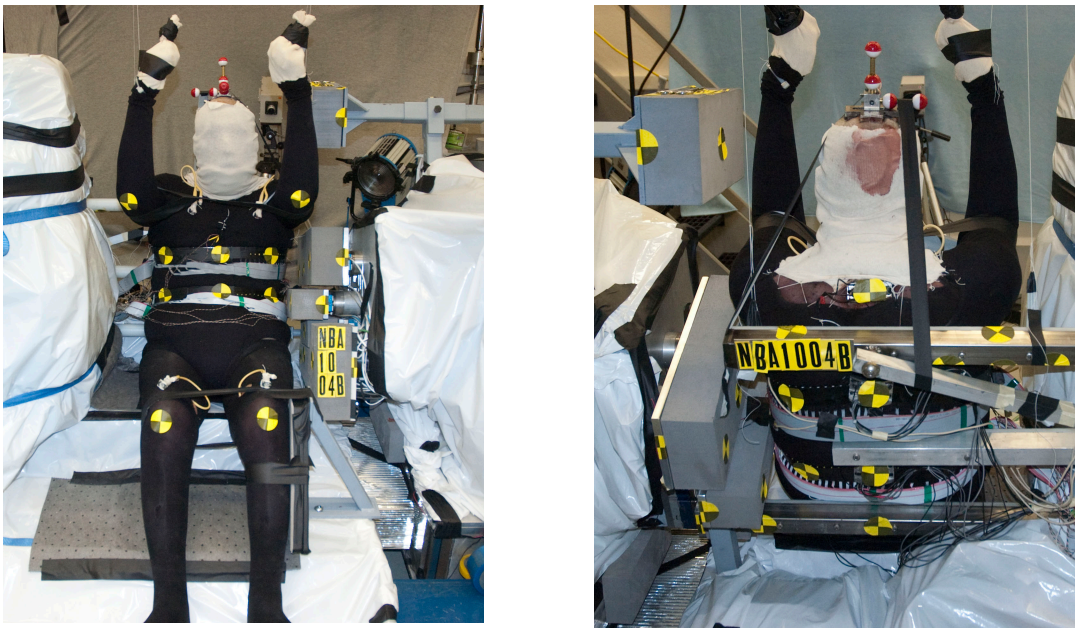

Figure 6. Front and rear pre-test images showing occupant posture and position.

To prevent interaction of the subject's arm and shoulder with the impactor wall, the upper extremities were positioned with the arms approximately horizontal or angled somewhat upward and above the thorax loading plate, and with the forearms vertical.

Data Collection and Processing

Data were recorded at a rate of 10 kHz using a combination of DTS TDAS Pro and G5 hardware (DTS, Seal Beach, CA). Data from the impact wall load cells, spine accelerometers, and pelvis accelerometers were filtered using SAE class 180 filters. Rib strain data and raw chestband data were filtered using SAE class 1000 filters.

Each impact event was recorded using multiple high-speed video cameras recording at a rate of 1000 frames per second. Contact between pieces of copper tape located on the abdomen and the impactor plate used to load the abdomen was used to produce a switch closure, which was recorded by data acquisition. The time at which this switch closure occurred was used to define tzero (i.e., 0 ms). LEDs activated by this switch closure were used to sync the high-speed camera images with the recorded transducer data.

Compression of the subject's thorax and abdomen was calculated from chestband contours using methods similar to those described by Pintar et al. (1997) and Maltese et al. (2002). As illustrated in Figure 7, reference lines between the spine anchor point and the most anterior point on the subject's thorax or abdomen were defined from undeformed (pre-impact) abdomen and thorax chestband contours. Changes in the perpendicular distances between these lines and a location on the chestband corresponding to the lateral margin of the impacted side of the contour in the undeformed condition were used to calculate half-chest and half-abdomen width and deflection.

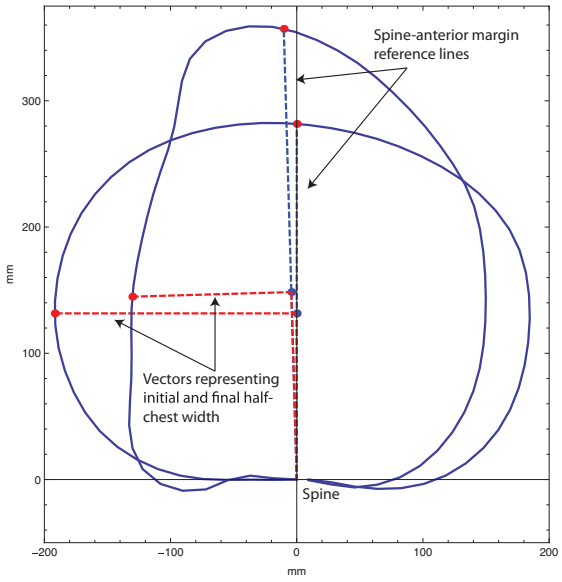

Figure 7. Illustration of the method used to calculate external deflection from chestband contours.

Mean and ± 1 SD response corridors were developed using methods described by Maltese et al. (2002). Prior to generating these corridors (which are henceforth referred to as response targets per NHTSA convention), subject responses were scaled using equal-stress, equal-velocity scaling based on 50th-percentile ATD mass (76 kg). For the 10-m/s tests, test NBA0901B was used as the reference condition for signal time shifting. For the 3- and 8-m/s tests, signal time shifting was performed using tests NBA1004A and NBA1004B as reference conditions, respectively.

Injury Documentation

As indicated above, subjects were CT scanned prior to testing and between the low and high-speed tests to identify injuries. Following the high-speed test, each subject was autopsied to document locations and types of injuries produced during the tests.

RESULTS

Injuries

Detailed descriptions of the injuries produced during each test are listed in Table 2, while detailed autopsy results for each subject are listed in Appendix B. A pre-test CT scan revealed that the subject used in test NBA0902A had pre-existing, non-displaced rib fractures. Because the focus of the current work was on the abdomen, the subject was tested but thorax responses from this subject were also excluded from all analyses. However, the abdomen and pelvis responses were used because the pre-existing thorax rib fractures were not likely to have affected the responses of these body regions.

Two of the seven 3-m/s tests produced rib fractures. The fractures in tests NBA0901A and NBA1107A were lateral and anterior-lateral and involved ribs 2 through 9 on the struck side of the subject. Non-displaced rib fractures were also observed on the side of the body that was impacted in the 3 m/s test of one other subject (NBA0903A) in the autopsy that occurred following test. Although these fractures were not visible in post-test CT, strain gage data from subsequent tests demonstrates that rib fractures that are not visible on CT can occur in low-speed tests and therefore, these fractures are thought to have occurred in test NBA0903A rather than in the subsequent high-speed test.

One of the three 8-m/s tests did not produce any injuries (NBA1004B), while the remaining 8-m/s tests resulted in three struck-side rib fractures (NBA1005B) and a single rib fracture to the struck side (NBA1006B). The two tests conducted at 10 m/s (NBA0901B and NBA0903B) resulted in numerous rib fractures that were posterior, posterior-lateral, lateral, and anterior-lateral on the struck-side of the body. Test NBA0903B also resulted in a grade-II spleen laceration.

Table 2. Injury Outcome for Low and High Severity Impacts

Test ID	Impact Speed	Impact Side (Right or Left)	Fx'd Ribs	Fractured Rib Locations			# Ribs Fx'd	# Rib Fxs	Other Injuries and Injury Info.	AIS Score (AAAM 2005, '08 update)
				Anterior	Lateral	Posterior				
NBA0901A	3 m/s	Right	R2*	NFS			5	6		450203.3
			R6	NFS						
			R7	NFS						
			R8		NFS					
			R9*	NFS	NFS					
NBA0901B	10 m/s	Left	L2	P			10	23	Flail chest	450213.4
			L3		C, NDS	C, NDS				
			L4	C, DS	C, NDS	C, NDS				
			L5	C, DS	C, NDS	C, NDS				
			L6	C, DS	C, NDS	C, NDS				
			L7	C, DS	C, NDS	C, NDS				
			L8	P	C, NDS	C, NDS				
			L9		C, NDS	C, NDS				
			L10		C, NDS	C, NDS				
			L11			C, DS				
NBA0902A	3 m/s	Left					0	0		
NBA0903A	3 m/s	Right	R5*		NFS		2	2		450202.2
			R6*		NFS					
NBA0903B	10 m/s	Left	L5			C, NDS	7	9	Grade II spleen laceration, mid-sternum fracture, Flail chest	450203.3 450804.2 544222.2
			L6		C, NDS	C, NDS				
			L7		C, NDS	C, NDS				
			L8			C, NDS				
			L9			C, NDS				
			L10			C, NDS				
			L11		C, NDS					
NBA1004A	3 m/s	Right					0	0		
NBA1004B	8 m/s	Left					0	0		
NBA1005A	3 m/s	Right					0	0		
NBA1005B	8 m/s	Left	L4	C, NDS			3	3	laxity in costo-sternal joint for left ribs 5 and 6.	450203.3
			L5	C, NDS						
			L6	C, NDS						
NBA1006A	3 m/s	Right					0	0		
NBA1006B	8 m/s	Left	L5		C, NDS		1	1		450201.1
NBA1107A	3 m/s	Left	L7		C, NDS		2	3		450202.2
			L8	C, NDS	C, NDS					

P: Partial NDS: Nondisplaced
C: Complete NFS: Not further specified
DS: Displaced * Timing of fracture inconclusive

Force Histories

Figure 8 shows the scaled applied force histories for the thorax, abdomen, iliac wing, greater trochanter, and mid thigh for the 3, 8, and 10 m/s test conditions. Also shown are the mean response and mean ± 1 standard deviation response targets defined from these curves. Because only two tests were performed at the 10 m/s condition, ± 1 SD response targets were not developed and the individual responses and the average response are plotted. Figure 8 also shows a plot containing the sum of the applied force histories to the pelvis (i.e., greater trochanter plus iliac wing forces) and ± 1SD response targets determined form these force histories at each impact speed. The maximum value of the mean scaled applied force for each of the five body regions subjected to the three test conditions are listed in Table 3.

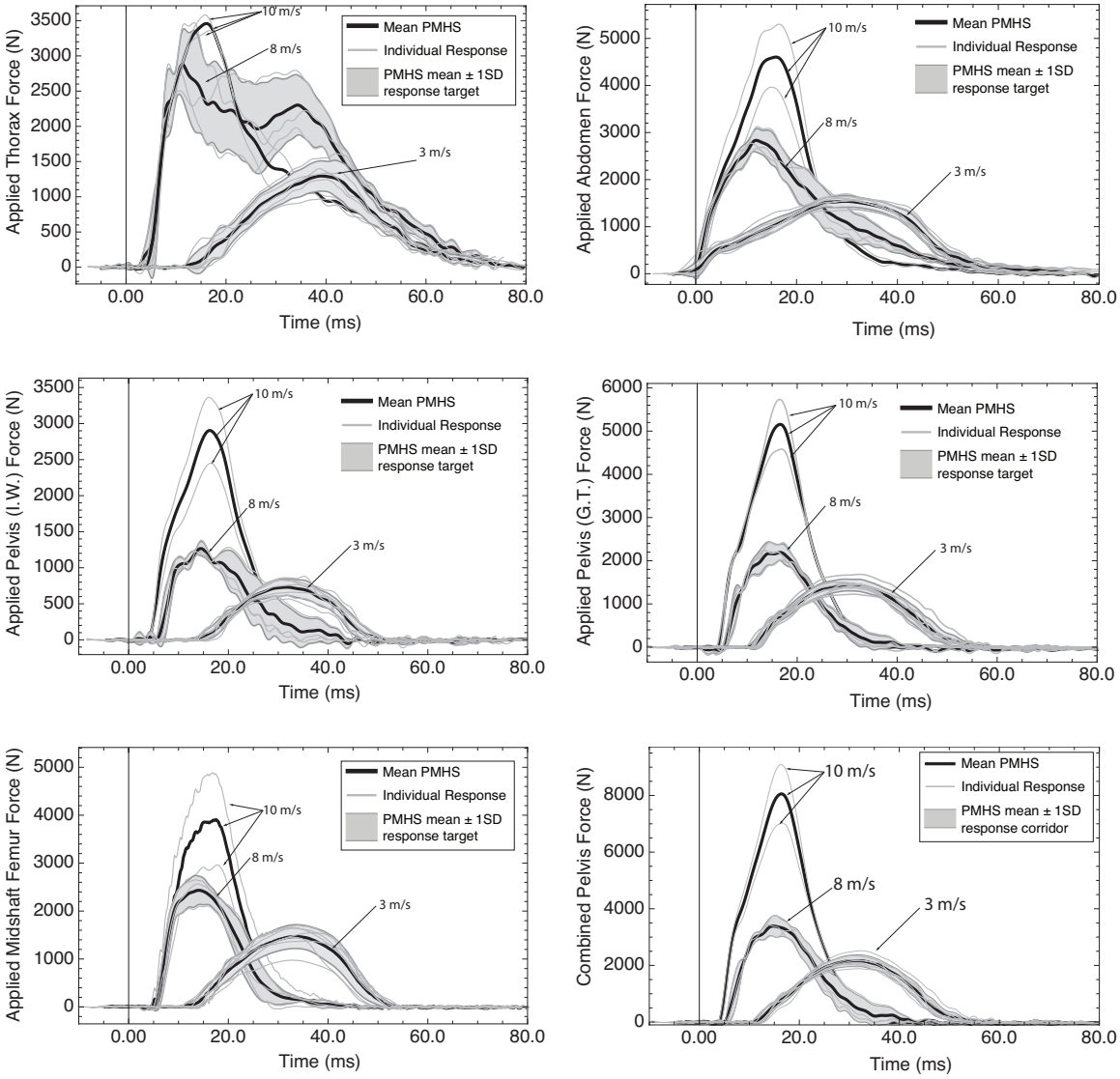

Figure 8. Scaled applied force histories for the thorax (top left), abdomen (top right), iliac wing (middle left), greater trochanter (middle right), mid-shaft femur (bottom left), and combined iliac wing and greater trochanteric forces (bottom right) for the 3-, 8- and 10-m/s tests.

Table 3. Peak Mean Scaled Applied Forces by Body Region and Test Condition

Body Region	3 m/s		8 m/s		10 m/s	
	Mean (kN)	SD	Mean (kN)	SD	Mean (kN)	Range
Thorax	1.3	0.22	2.9	0.49	3.5	3.4 - 3.6
Abdomen	1.5	0.13	2.8	0.25	4.6	3.9 - 5.3
Iliac Wing	0.7	0.12	1.3	0.10	2.9	2.4 - 3.4
Greater Trochanter	1.4	0.14	2.2	0.19	5.2	4.5 - 5.7
Mid-Shaft Femur	1.5	0.25	2.4	0.30	3.9	2.9 - 4.9

Spine Accelerations

Scaled spine Y-axis accelerations measured at the subject's upper-thorax spine, mid-thorax spine, and mid-lumbar spine for the 3-, 8-, and 10-m/s tests are shown in Figure 9. In general, the acceleration of the mid-lumbar spine leads the acceleration of the thorax-spine due to the offset of the abdomen section of the impact wall.

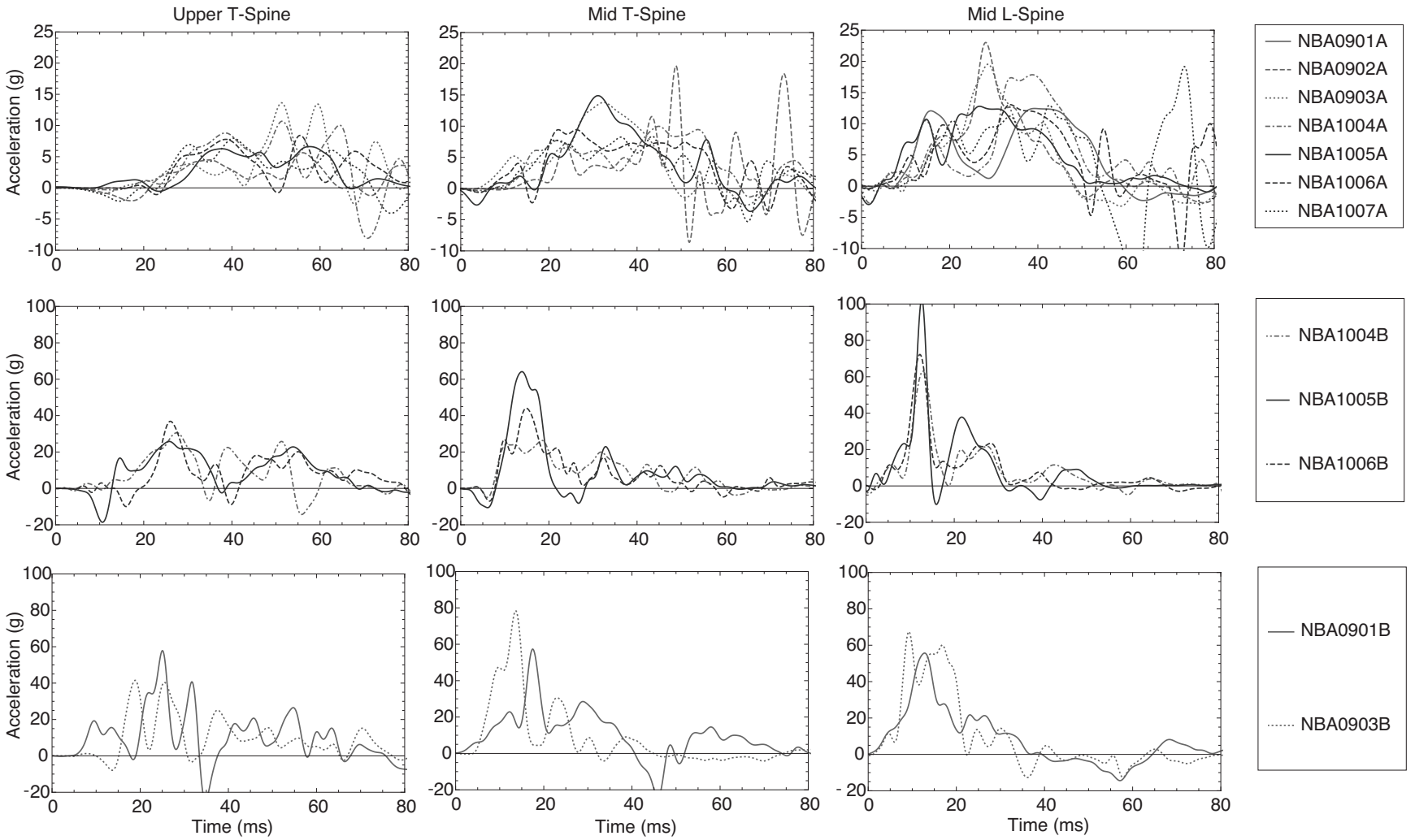

Figure 9. Scaled lateral accelerations of the upper-thorax, mid-thorax, and mid-lumbar spine for the 3 m/s (top row), 8 m/s (middle row), and 10 m/s (bottom row) test conditions.

Pelvis Accelerations

The pelvis lateral (Y-axis) acceleration histories for the 3-, 8-, and 10-m/s tests are shown in Figure 10. Also shown are the mean ± 1 SD response targets for the 3- and 8-m/s tests, as well as the mean response for the three test conditions. Table 4 lists the peak values of the mean scaled lateral pelvis accelerations for the three test severities.

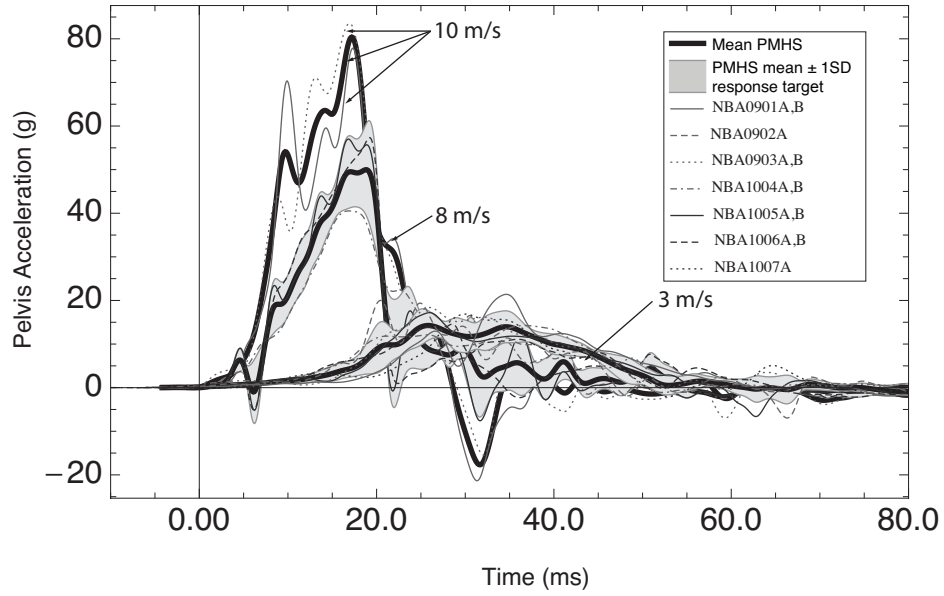

Figure 10. Scaled pelvis Y-axis acceleration histories for 3-, 8-, and 10-m/s tests.

Table 4. Peak Mean Scaled Pelvis Accelerations

Test Condition	Pelvis Acceleration (*g*)
3 m/s	14
8 m/s	50
10 m/s	80

External Deflections

The external deflection histories of the thorax for the 3- and 8-m/s test conditions and the associated ±1 SD response targets are shown in Figure 12. The 3 m/s thorax responses in Figure 11 do not include results from test NBA0901A because the thorax plate contacted the part of the arm in this test, making comparisons with subsequent tests difficult. Deflection from test NBA0902A is also excluded from Figure 11 because the subject used in this test had pre-existing thoracic rib fracture that invalidated thoracic force and deflection measurements.

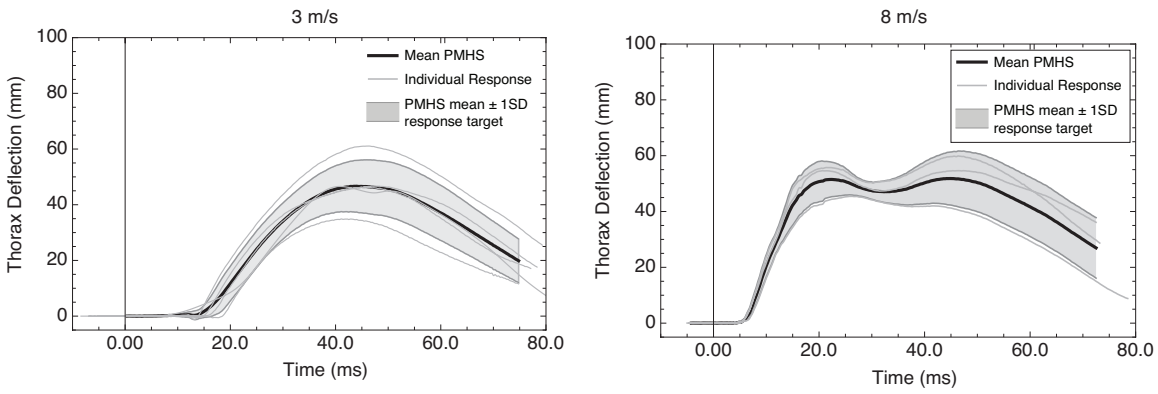

Figure 11. Scaled external thorax deflection histories for the 3- and 8-m/s tests.

External abdomen deflection histories from individual tests and mean abdomen deflection response are shown in Figure 12 for each of the test conditions. Also shown are the response targets for the 3- and 8-m/s tests. A mean abdomen deflection response is shown in Figure 12 for the two 10 m/s tests up to 20 ms, at which time the abdomen chestband failed in one of the tests. The peak mean values of the scaled external thorax and abdomen deflections are listed in Table 5. Chestband contours from each test showing the initial contour and the contour at the time of peak defection are shown in Appendix B.

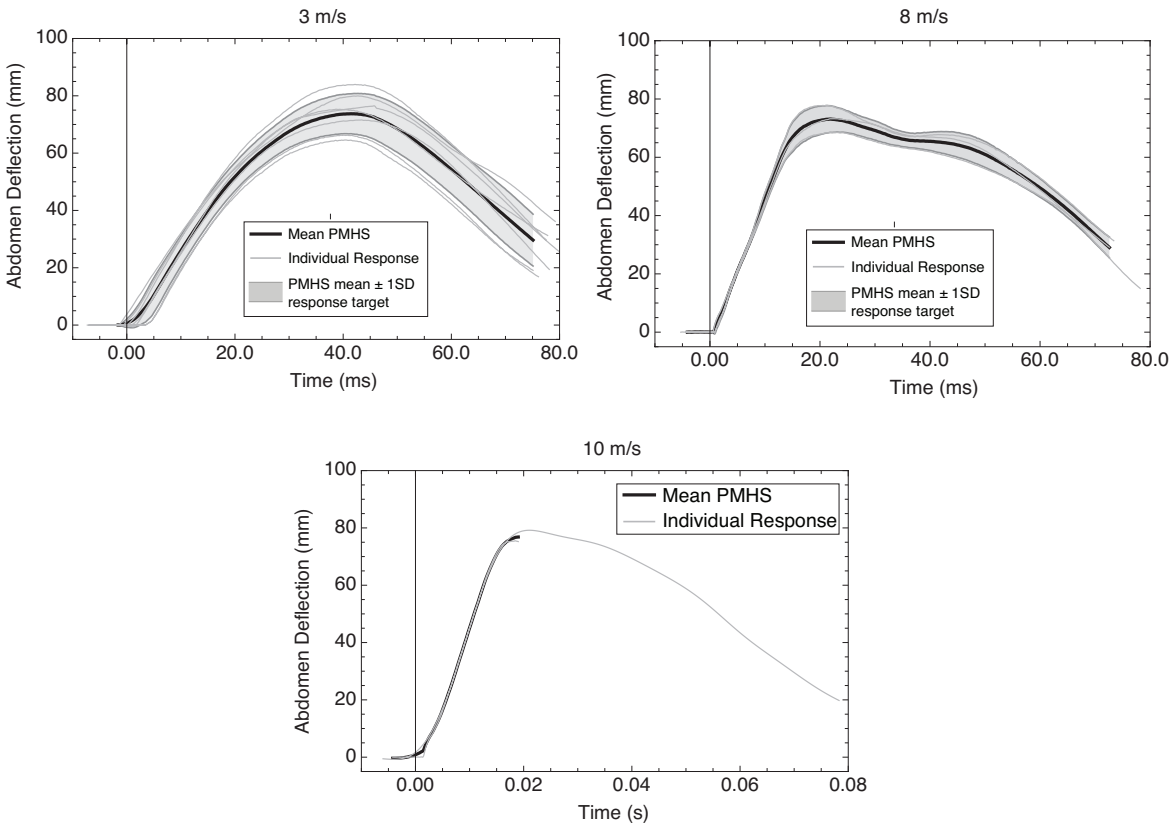

Figure 12. Scaled external abdomen deflection histories for the 3, 8, and 10 m/s test conditions.

Table 5. Mean Peak Scaled External Thorax and Abdomen Deflections

Test Condition	External Thorax Deflection (mm)	External Abdomen Deflection (mm)
3 m/s	47	74
8 m/s	54	75
10 m/s	NA	77

Force-Deflection Responses

Scaled thorax force-deflection curves for the 3- and 8-m/s tests conditions and scaled abdomen force deflection curves from the 3-,8, and 10-m/s tests are shown in Figure 13. Deflections are from the mid-thorax and abdomen chestbands. Scaled applied forces are from loads measured by the thorax and abdomen sections of the impact wall. Peak abdomen deflection did not change with impactor velocity, but peak force applied to the abdomen increased substantially with impact velocity, indicating that the abdomen response is highly rate-sensitive.

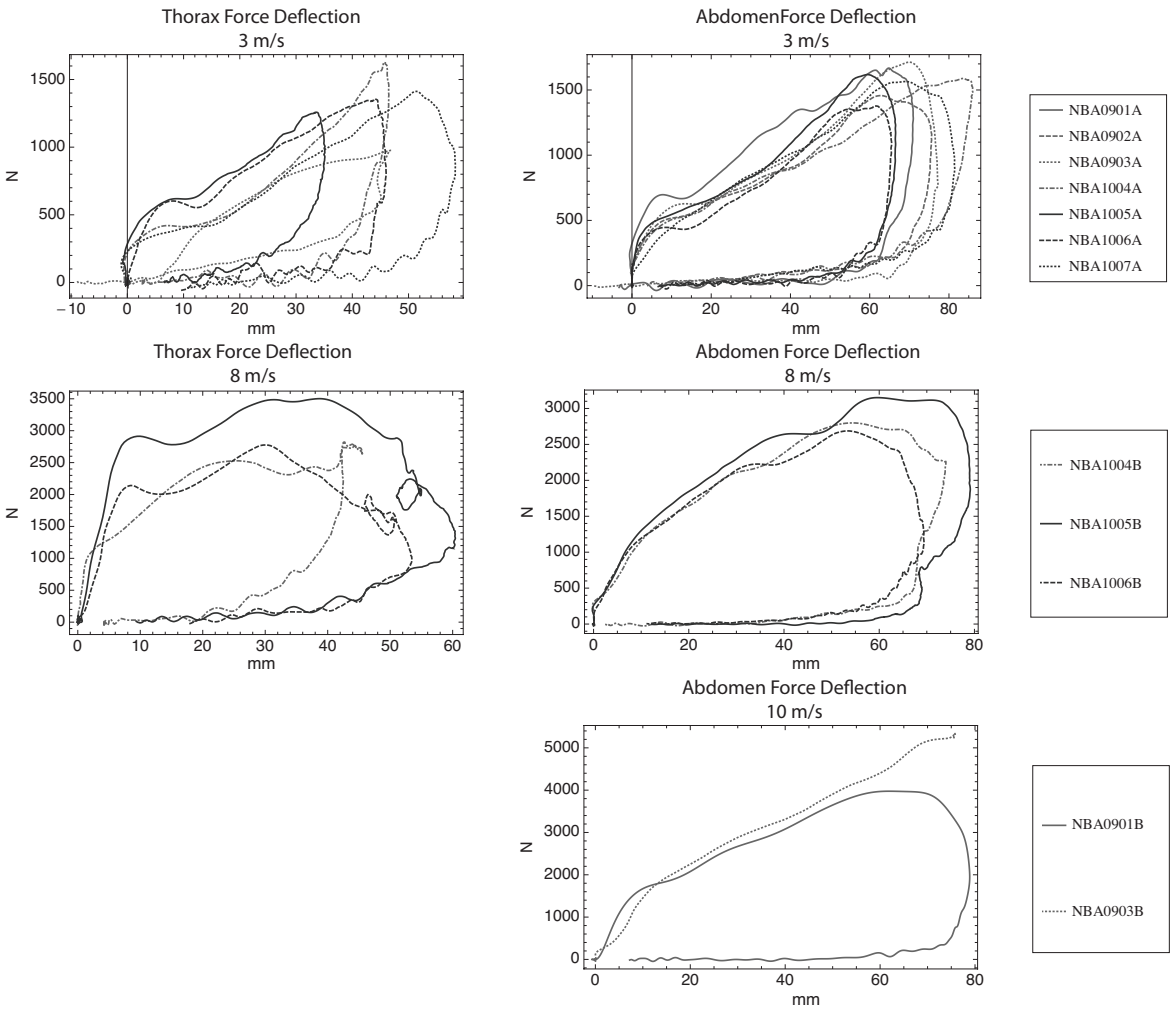

Figure 13. Scaled external thorax force-deflection responses for the 3- and 8-m/s test conditions and scaled external abdomen force-deflection responses from the 3-, 8-, and 10-m/s tests conditions created using scaled force and scaled deflection data.

DISCUSSION

This study provides new data on human lateral-impact response that are needed to assess the biofidelity of current side-impact crash test dummies and to develop improved computational models. Data from the seven subjects tested at a 3-m/s impact speed have more than doubled the number of low-severity, whole-body, lateral impact tests in the biomechanical literature. Separate measurements of force applied to the iliac wing and greater trochanter obtained in this study provide the first data on load sharing between pelvic components measured in a whole-body sled test. This study is also the first to use whole-body sled tests to replicate the decrease in door intrusion velocity that occurs in real-world side impacts as the struck vehicle decelerates and the striking vehicle accelerates. Importantly, the current study provides new data on the force-deflection response of the lower abdomen to lateral impact that are needed to assess the performance of current side-impact ATDs.

Prior to this study, no data on the response of the mid thigh were available, since all previous whole-body, side-impact tests did not separately load the mid thigh and instead used a pelvis plate that covered the pelvis and part of the thigh. As a result, using data from previous tests to define side impact ATD pelvis response does not ensure correct load sharing between the pelvis and the thigh, which is required for appropriate assessment of pelvis injury potential. In contrast to previous studies, the current study separately loads the thigh and thereby provides data that define load sharing between the pelvis and thigh.

Rib fracture patterns produced in the current study followed generally accepted patterns for pure lateral impact to nearside occupants (Pintar et al. 1997). For the 3-m/s and 8-m/s tests, rib fractures were located at lateral, anterior-lateral, and posterior-lateral regions of the ribcage on the struck side of the body. In the 10-m/s tests, fractures were located at posterior, lateral, and anterior-lateral regions of the ribcage on the struck side.

The impactor padding force-deflection characteristics and the 10-m/s and 8-m/s velocity profiles used in this study were selected to replicate door velocity histories and ATD responses from a subset of SNCAP tests of passenger vehicles conducted between 1998 and 2004. Because many of these vehicles did not have side-impact airbags, the padding in the thorax portion of the impactor does not account for the cushioning effect provided by side-impact airbags and the thorax responses measured in this study are not representative of thorax responses produced for nearside occupants in vehicles with side-impact airbags.

Limitations

The use of a padded impactor with a fixed abdomen offset and impactor velocity history that decreased after initial occupant contact in 8-m/s and 10-m/s tests results in loading conditions for the abdomen that are representative of that which occurs in side NCAP crash tests. However, the use of such loading conditions may confound the measurement of responses of the thorax and pelvis. In particular, decreasing door velocity during subject loading coupled with a fixed-shape impactor means that differences in subject body shape (such as variations in pelvic breadth) can result in differences in the impactor

velocity at the time at which it contacts the pelvis and thorax between subjects. While such differences are expected in real-world side impacts, these differences confounded the measurement of thorax and pelvic responses in the current test series by changing the loading condition that the thoraces and pelves of different subjects sustained in the 8 m/s and 10 m/s tests. However, the difference in pelvis and thorax contact timing between subjects for similar body regions in the 8-m/s and 10-m/s tests were typically less than 2 ms, which corresponds to an approximately 0.4 m/s difference in impactor speed at the time of contact. Further, the responses measured in the 3-m/s tests are not as affected by differences in subject shape as the higher-speed tests because the 3 m/s tests used an impactor velocity that did not decrease while the occupant was being loaded.

Chest and abdomen deformation were measured using chestbands that were constrained so that a portion of the band was fixed to the spine and so that the total circumference of the band was constant. As a result, the band was capable of constraining the circumferences of the thorax and abdomen in a manner that could have affected the deformations of these body regions. In particular, for the abdomen, the use of a fixed-circumference chestband probably resulted in more out-of-plane motion of abdomen tissues than would have occurred if the band were not used, or if the circumference of the chestband were not constrained.

For tests where rib fractures occurred, rib fracture timing is generally unknown because only a few of the strain gages were located at or near a rib fracture. As a result of this, any future analyses that use the data collected in this study to establish relationships between mid thorax and lower thorax/upper abdomen deformation and injury should likely treat deflection data as censored. That is, the rib fractures likely occurred at a deflection less than the maximum deflection observed. Rib fracture timing was also unknown for the 10-m/s tests and multiple bilateral rib fractures were produced in these tests. Consequently, caution should be used in interpreting the thoracic response data from the 10 m/s tests.

Although previous studies tested cadavers using an arm position that was nominally vertical (e.g., Irwin et al. 1993 and Pintar et al. 1997), the current study used a less realistic, horizontal arm orientation. This approach was necessary to ensure the fidelity of the abdomen force and deflection measurements by prevent the arm from interacting with the abdomen plate.

Similar to some previous NHTSA lateral impact cadaver tests (e.g., Pintar et al. 1997) the impactor used in this study did not engage the shoulder. This loading condition is more representative of the loading condition produced in side impact crash tests of vehicles produced in the early to mid 2000's model vehicle and less like the loading conditions produced in side impact tests of many current model vehicles, which generally have higher door panels and thus are more likely to engage shoulder. Although less representative of the loading condition of current vehicles, not engaging the shoulder simplified and improved the repeatability of the loading conditions for the thorax and abdomen.

Comparisons with Previous Studies

Comparisons between the abdomen and pelvis responses from the 10 m/s and 8 m/s tests in this study and similar responses measured in previous, Heidelberg-style side impact tests performed using flat, padded impact walls are shown in Figure 15 through Figure 19. Comparisons between thorax responses from previous studies and thorax responses measured in the current study were not made because thorax loading conditions in the current study were substantially different from those used in previous studies. In particular, padded impacts performed in previous whole-body sled tests loaded the thorax through the arm (e.g., Irwin et al. 1993, Pintar et al. 1997), whereas the current study directly loaded the thorax with a padded impactor. These differences in arm position have been shown to affect thorax response, rib strain, and rib fracture patterns in side impact (Kemper et al. 2008). These differences may also affect the comparability of abdominal responses between the current study and previous studies.

Figures 14 through 16 compare the 8-m/s response targets and 10-m/s responses for force applied to the abdomen, force applied to the pelvis, and abdomen deflection from the current study to response targets developed from the results of previous Heidelberg-style whole body side impact tests conducted using a flat, padded impact wall and impact speeds of 6.7 m/s and 8.9 m/s (ISO TR9790, Maltese et al. 2002). Despite differences in impact speed and impact wall shape between the current study and previous Heidelberg-style tests, the abdomen responses from the current study exhibit the expected trends. That is, peaks from the10-m/s abdomen responses from the current study are either above or within 8.9 m/s abdomen response targets from previous studies and the 8 m/s response targets from the current study are above or within the 6.7 m/s response targets for similar measurements from previous studies. As expected, because impactor velocity decreased during abdomen loading, the durations of the response targets for force applied to the abdomen from the current study were ~10 ms shorter than the durations of the ISO TR9790 abdomen force corridors or the Maltese et al. target responses for abdomen force. However, the durations of the abdomen deflection response targets from the current study were similar those of in ISO TR9790 and Maltese et al. for similar responses, possibly because of hysteresis in the foam padding on the abdomen plate and the hysteresis in the abdomen itself.

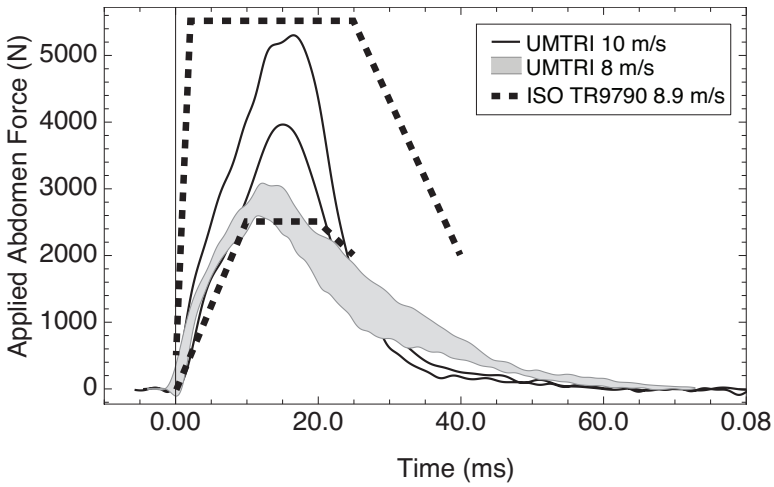

Figure 14. Midsize male 8-m/s response target and 10-m/s responses for force applied to the abdomen compared to response targets for abdomen force from padded impacts with a flat wall at 8.9 m/s from ISO TR9790.

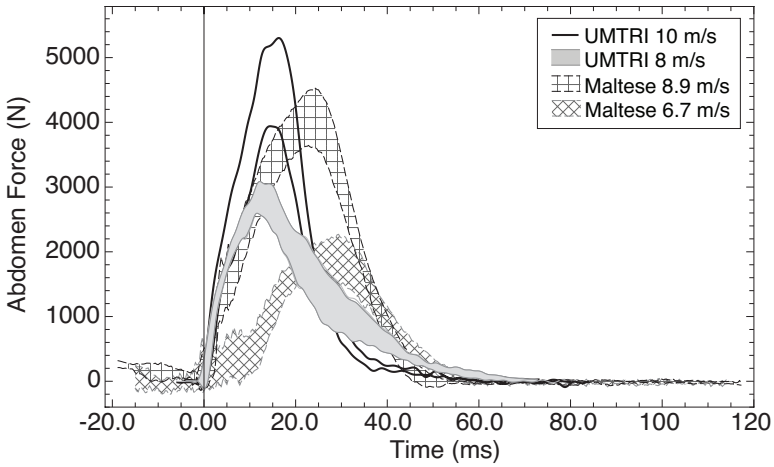

Figure 15. Midsize male 8-m/s response target and 10-m/s responses for force applied to the abdomen compared to response targets for abdomen force from padded impacts with a flat wall at 6.7 m/s and 8.9 m/s developed by Maltese et al. (2002).

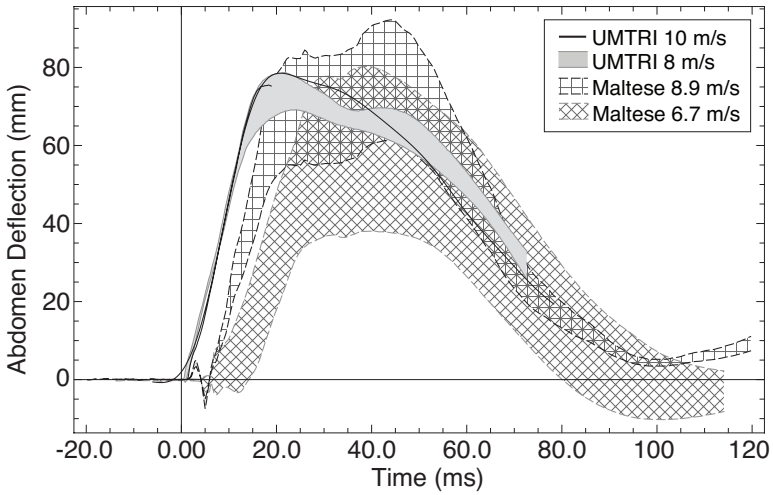

Figure 16. Midsize male 8-m/s response target and 10-m/s responses for abdomen deflection compared to response targets for abdomen deflection from padded impacts with a flat wall at 6.7 m/s and 8.9 m/s developed by Maltese et al. (2002).

Figures 17 and 18 compare pelvis lateral acceleration response targets and pelvis force response targets for 6.7 m/s and 8.9 m/s padded impacts developed by Maltese et al. to the 8-m/s response target and 10-m/s responses for similar quantities from the current study. The 8 m/s and 10 m/s pelvic response targets had a shorter duration than response targets generated by Maltese et al., likely because impactor velocity was constant during impact in the studies analyzed by Maltese et al., while impactor velocity decreased while the subject was being loaded in the current study. The pelvis force response target from the current study for the 8 m/s loading condition, determined by summing iliac wing and greater trochanter forces, was below the 6.7 m/s pelvis force response target developed by Maltese et al. Consistent with this trend, the 10 m/s pelvis force responses were either within or below the Maltese et al. 8.9 m/s pelvis force response target. The higher pelvic forces produced in the tests analyzed by Maltese et al. may be from the use of stiffer padding, or because the plate that loaded the pelvis in the studies analyzed by Maltese et al. was large enough so that it may have caught part of the thigh in addition to the pelvis.

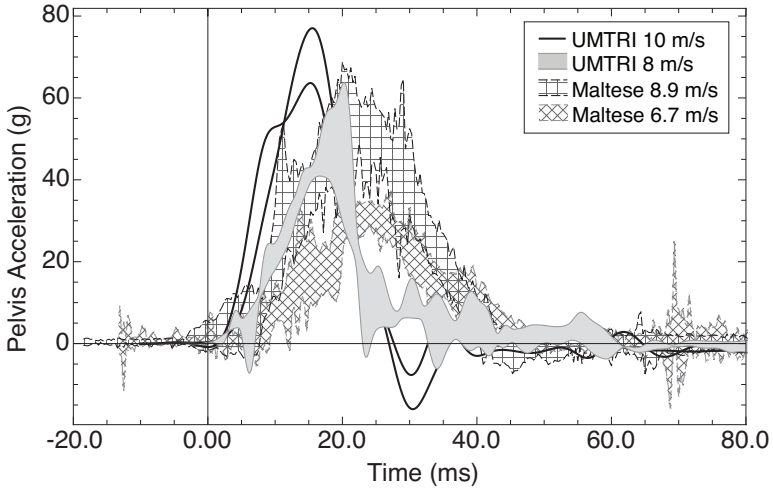

Figure 17. Midsize male 8-m/s response target and 10-m/s responses for pelvis Y-axis acceleration compared to response targets for pelvis Y-axis acceleration from padded impacts with a flat wall at 6.7 m/s and 8.9 m/s developed by Maltese et al. (2002).

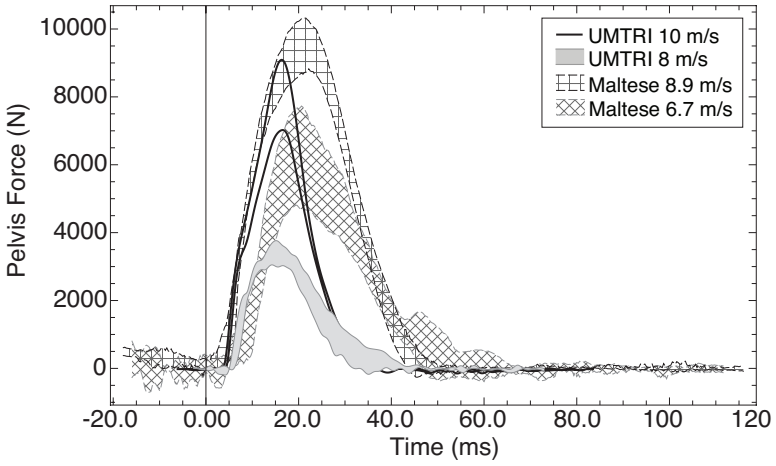

Figure 18. Midsize male 8-m/s response target and 10-m/s responses for pelvis force (sum of greater trochanter and iliac wing forces) compared to response targets for pelvis force from padded impacts with a flat wall at 6.7 m/s and 8.9 m/s developed by Maltese et al. (2002).

The current study provides the first data on load sharing between the iliac wing and greater trochanter measured in a whole-body sled test. However, Bouquet et al. (1998) previously reported on load sharing between the iliac wing and greater trochanter in a series of pendulum lateral impacts to the pelves of 10 cadavers with impact velocities ranging from 9.47-13.7m/s. Table 6 compares the proportion of force applied to the pelvis that was transmitted to the greater trochanter at the time of peak force in the current study to a similar quantity reported by Bouquet et al. (1998). Based on a t-test, there are no significant differences between the results reported by Bouquet et al. and those of the current study at either the 3-m/s or 8-m/s loading conditions ($p=0.5$ for 3-m/s data and $p=0.2$ for 8-m/s data).

Table 6. Percentage of Pelvic Force Applied to the Greater Trochanter at the Time of Peak Pelvic Force

Test Series ID	3 m/s	8 m/s	10 m/s
NBA0901	65%		63%
NBA0902	62%		
NBA0903	67%		65%
NBA1004	65%	61%	
NBA1005	73%	65%	
NBA1006	70%	63%	
NBA1007	63%		
Mean±SD	*66%±4%*	*63%±2%*	*64%*
Bouquet et al. Mean±SD		*68%±7%*	

CONCLUSIONS

New data on the lateral-impact response of the body, and particularly of the abdomen, to nearside-occupant loading conditions were collected using low-severity impacts and higher severity impacts that represent door-to-occupant loading velocity profiles that occur in FMVSS 214 side-impact tests. Results of this study provide human response targets that define the force-deflection response of the lower abdomen and the impact response of the thigh, iliac wing, and greater trochanter that can be used to assess and if necessary, tune the side-impact responses of ATD and human computational models.

REFERENCES

Bendjellal, F., Walfish, G., & Fayon, A., and Tarriere, C. (1984). APR biomechanical data. Nanterre, FR: Association Peugeot-Renault.

Bouquet, R., M. Ramet, F. Bermond, Y. Caire, Y. Talantikite, S. Robin, and E. Voiglio (1998). Pelvis human response to lateral impact. In: Proceedings of the 16th International Technical Conference on the Enhanced Safety of Vehicles. Windsor, Ontario, Canada:, U.S. Department of Transportation, Washington, DC, pp. 1665–1686.

Cavanaugh, J. M., Walilko, T. J., Malhotra, A., Zhu, Y., & King, A. I. (1990a). Biomechanical Response and Injury Tolerance of the Thorax in Twelve Sled Side Impacts. SAE 902307 in Proceedings of the Thirty-fourth Stapp Car Crash Conf. Warrendale, PA, US: Society of Automotive Engineers.

Cavanaugh, J. M., Walilko, T. J., Malhotra, A., Zhu, Y., and King A. I., 1990b, "Biomechanical Response and Injury Tolerance of the Pelvis in Twelve Sled Side Impacts," SAE 902305, Proceedings of the Thirty-fourth Stapp Car Crash Conf., P-236, Society of Automotive Engineers, Warrendale, PA.

Cesari, D. Compigne, S., Scherer, R., Xu, L., Takahashi, N. et al. (2001). WorldSID Prototype Dummy Biomechanical Responses. Stapp Car Crash J 45:1-34.

Eppinger, R. H., Augustyn, K., & Robbins, D. H. (1978). Development of a Promising Universal Thorax Trauma Prediction Methodology. SAE 780891 in Proceedings of the 22nd Stapp Car Crash Conference. Warrendale, PA, US: Society of Automotive Engineers. Pages 209-268.

Hallman J.J., Yoganandan, N, and Pintar, F.A. (2010). Biomechanical and Injury Response to Posterolateral Loading from Torso Side Airbags. Stapp Car Crash J 54:227-257.

Irwin, A.L., Waliko. T.J., Cavanaugh, J.M., Zhu, Y., and King, A.I. (1993). Displacement Responses of the Shoulder and Thorax in Lateral Sled Impacts. Proceedings of the 37th Stapp Car Crash Conference, pp 165-173. Society of Automotive Engineers, Warrendale, PA.

ISOTR9790. (1999) Road vehicles-lateral impact response requirements to assess the biofidelity of the dummy. Technical Report No. 9790, International Standards Organization, American National Standards Institute, New York, NY.

Kallieris D., Mattern R., Schmidt G., and Eppinger R.H. (1981). Quantification of side impact responses and injuries. Proc. 25th Stapp Car Crash Conference, pp.329-366. Society of Automotive Engineers, Warrendale, PA.

Kallieris, D., Boggasch, F., Mattern, R. (1994). Protection for the Thorax Injury Severity in the 90-degree Lateral Collision. Paper 94-S1-0-02. Proceedings of the 14th

International Technical Conference on the Enhanced Safety of Vehicles. National Highway Traffic Safety Administration, Washington DC.

Kemper, A.R., McNally C, Kennedy E.A., Manoogian S.J., and Duma S.M. (2008). The Influence of Arm Position on Thoracic Response in Side Impacts. Stapp Car Crash J 52:379-340.

Klinch, K.D., Flannagan, C.A.C, Nicholson, K., Schneider, L.W. and Rupp, J.D. (2008). Abdominal injury in motor-vehicle crashes. Report UMTRI-2008-40. University of Michigan Transportation Research Institute, Ann Arbor, MI.

Kuppa, S., Eppinger, R.H., McKoy, F., Nguyen, T., Pintar, F.A., and Yoganandan, N. (2003). Development of Side Impact Thorax Injury Criteria and Their Application to the Modified ES-2 Dummy with Rib Extensions (ES-2re). Stapp Car Crash J 47:189-210.

Lessley, D., Shaw, G., Parent, D., Arregui-Dalmases, C. Kindig, M, et al. (2010). Whole-Body Response to Pure Lateral Impact. Stapp Car Crash J 54:289-336

Maltese, M., Eppinger, R., Rhule, H., Donnelly, B., Pinatr, F., & Yoganandan, N. (2002). Response targets of human surrogates in lateral impacts Stapp Car Crash J, 46, 321-351.

Petitjean A., Trosseille, X., Petit, P, Irwin, A, Hassan, J, and Praxl, N. (2009). Injury Risk Curves for the WorldSID 50th Male Dummy. Stapp Car Crash J 53:433-476.

Pintar, F. A., Yoganandan, N., Hines, M. H., Maltese, M. R., McFadden, J., Saul, R., Eppinger, R., et al. (1997). Chestband Analysis of Human Tolerance to Side Impact. Warrendale, PA: SAE International.

Rouhana, S.W. (2002). Biomechanics of Abdomen Trauma in *Accidental Injury Biomehcanics and Prevention*. Eds. Melvin, J.W. and Nahum, A.M. Springer-Verlag, New York, New York.

Shaw, J.M., Herriott, R.G., McFadden, J.D., Donnelly, B.R., and Bolte, J.H (2006). Oblique and Lateral Impact Response of the PMHS Thorax. Stapp Car Crash J 50:147-167.

Shaw, G., Bolton, J., Lessley, D., Parent, D., Riley, P., Crandall, J. (2010). Improved Method to Record the Response of Seated Live Human Surrogates in a Simulated Side Impact. Proceedings of the 2010 JSAE Annual Congress, Paper 455-20105080.

Viano, D. C. (1989). Biomechanical Responses and Injuries in Blunt Lateral Impact. SAE 892432 in Proceedings of the 33rd Stapp Car Crash Conference. Warrendale, PA, US: Society of Automotive Engineers.

Walfisch, G; Fayon, A; Tarriere, C; Rosey, JP; Guillon, F; Got, C; Patel, A; Stalnaker, R.L (1980) Designing of a dummy's abdomen for detecting injuries in side impact collisions. *Proceedings of the 1980 International IRCOBI Conference on the Biomechanics of Impacts*, pp. 149 – 164. IRCOBI, Bron, France.

Yang, S., Hagiwara, S., Engelke, K., Dhillon, M.S., Guglielmi, G., Bendavid, B.A., Soejima, O., Nelson, D.L., and Genant, H.K. (1994). Radiographic absorptiometry for bone mineral measurement of the phalanges: Precision and accuracy study. Radiology, 192: 857-859.

Yoganandan, N., Pintar, F.A., Stemper, B.D., Gennarelli, T., and Weigelt, J.A. (2007) Biomechanics of side impact: injury criteria, aging occupants, and airbag technology. J Biomech 40(2):227-243.

Yoganandan N., Pintar F.A., Humm, J.R., Hallman, J.J., and Maiman, D.J. (2011). Analytical And Experimental Data Of Chest Deflections And Injuries In Side Impacts. Proceedings of the 22nd International Technical Conference on the Enhanced Safety of Vehicles. Paper 11-0256. Available from <www-esv.nhtsa.dot.gov>

APPENDIX A – PADDING FORCE-DEFLECTION CHARACTERISTICS

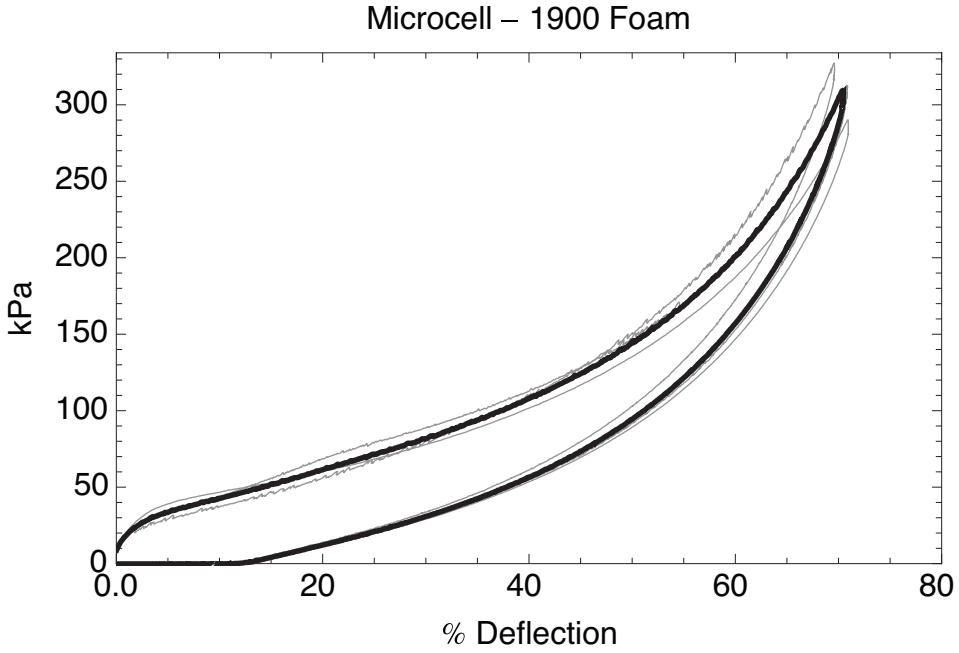

Figure A1. Compression deflection characteristics of Microcell 1900 polyolefin foam (Cellect, Johnsville, NY). Test specimen 50.8 by 50.8 by 25.4 mm, compression rate 12.5 mm/min.

Table A1. Pressure-deflection properties of Microcell 1900 polyolefin foam.

Properties	Test Method	Unit of Measure	Microcell 1900
Comp. Def @25%	ASTM-D-3575	kPa	72
Comp. Def @50%	ASTM-D-3575	kPa	145
Comp. Def @65%	ASTM-D-3575	kPa	235

APPENDIX B – INJURIES AND CHESTBAND RESPONSES

NBA0901

Subject: Male, 86 years, 77 kg

NBA0901A: 3 m/s (initial impact, RHS)

Thorax deflection:	n/a
Abdomen deflection:	72 mm
Injuries:	Right 2nd, 6th, 7th, and 9th anterior-lateral rib fx and right 8th and 9th lateral rib fractures. (Timing of right 2nd and 9th rib fxs inconclusive)

NBA0901B: 10 m/s (second impact, LHS)

Thorax deflection:	n/a
Abdomen deflection:	79 mm
Injuries:	10 left ribs fractured (23 rib fractures), flail

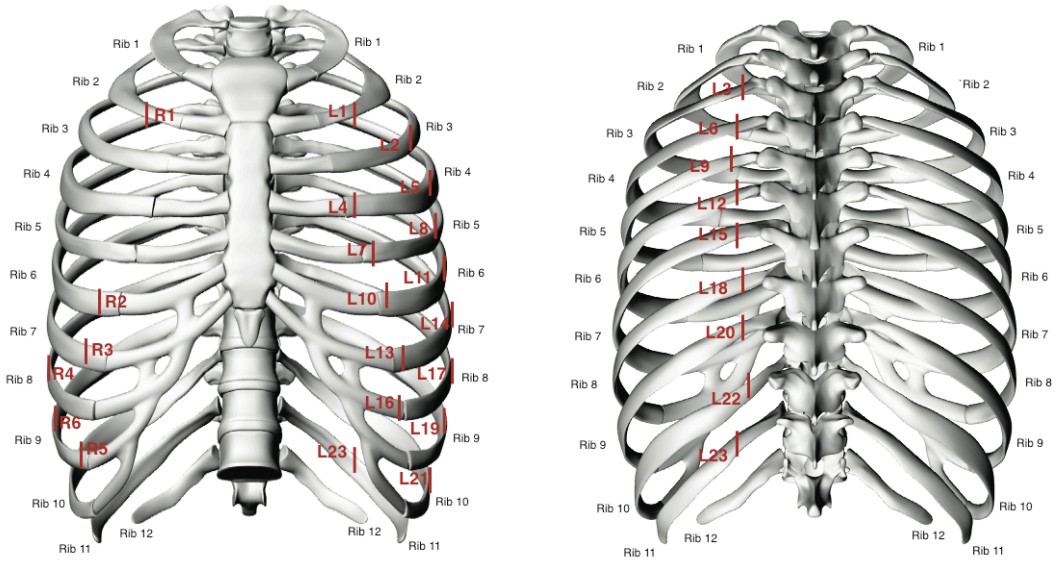

Figure B1. Locations of rib fractures as determined from NBA0901A post-test CT scan (ribs 6, 7, and 8) and NBA0901B post-test autopsy (all others).

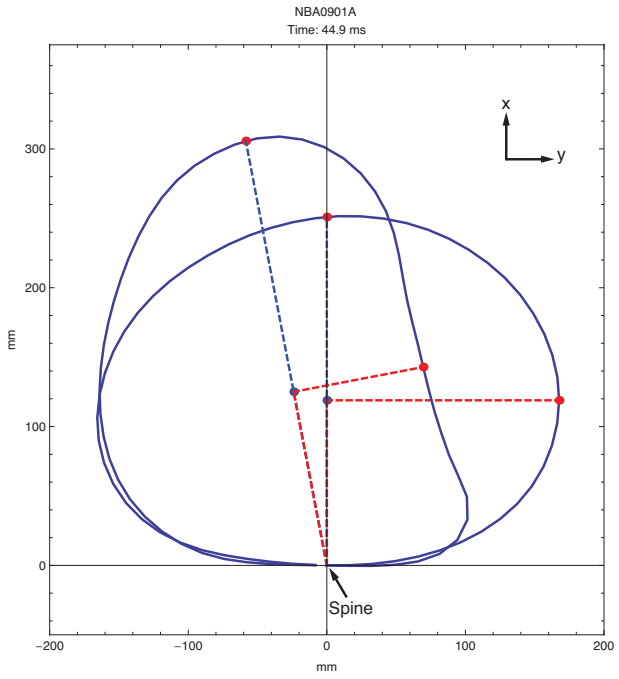

Figure B2. NBA0901A abdomen chestband contour.

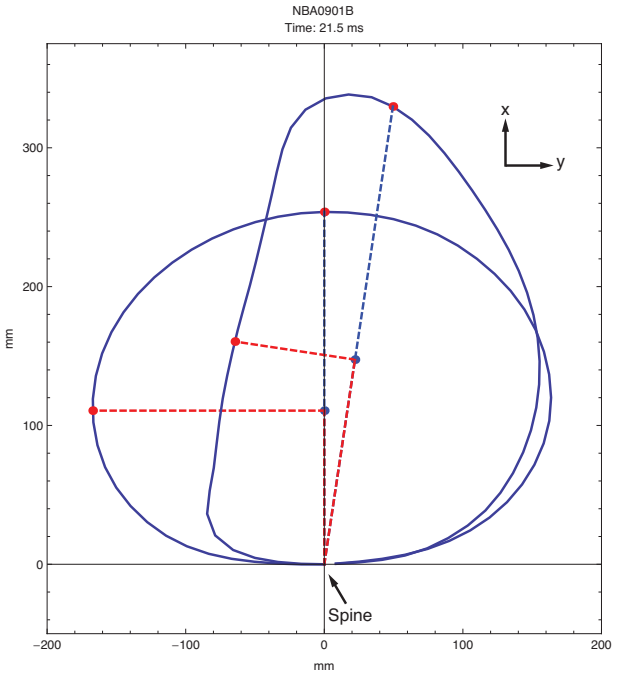

Figure B3. NBA0901B abdomen chestband contour.

NBA0902

Subject: Male, 61 years, 82 kg

NBA0902A: 3 m/s (initial impact, LHS)

Thorax deflection:	n/a
Abdomen deflection:	80 mm
Injuries:	a *pre-existing* rib fractures (8 total, all above abdomen). No abdominal injuries. No additional rib fractures

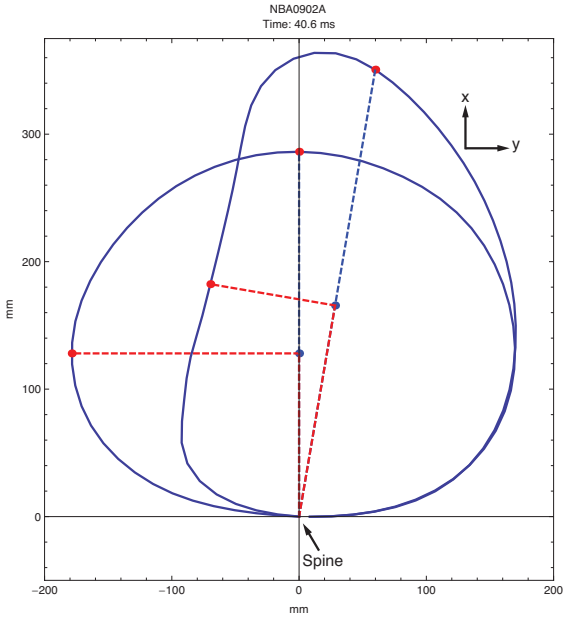

Figure B4. NBA0902A abdomen chestband contour.

NBA0903

Subject: Male, 50 years, 64 kg

NBA0903A: 3 m/s (initial impact, RHS)

Thorax deflection:	42 mm
Abdomen deflection:	69 mm
Injuries:	Right 5th and 6th lateral rib fxs

NBA0903B: 10 m/s (second impact, LHS)

Thorax deflection:	n/a
Abdomen deflection:	72 mm
Injuries:	7left ribs fx'd (9 rib fxs), grade II spleen laceration, mid sternum fracture

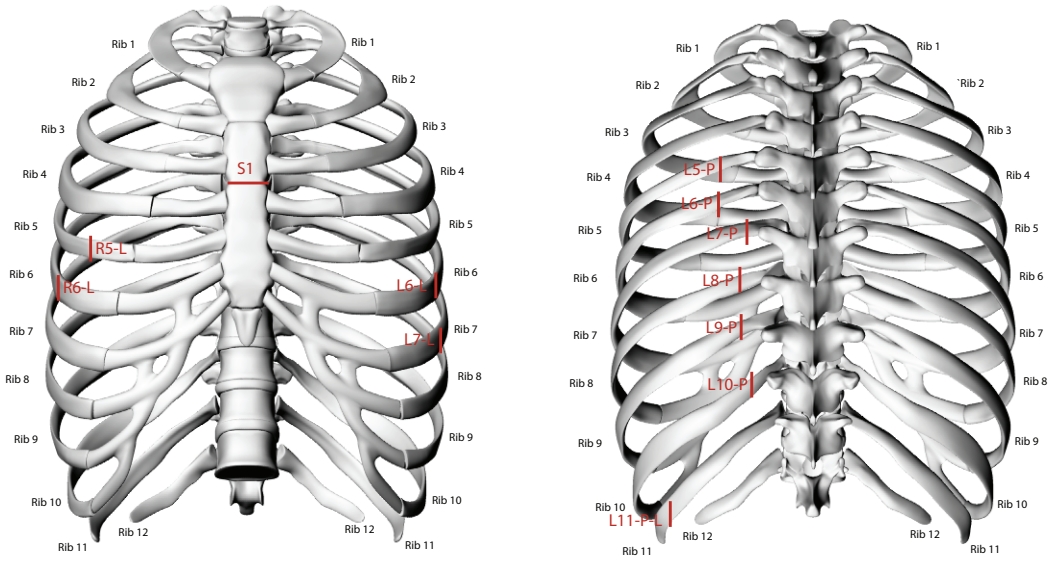

Figure B5. Locations of rib fractures as determined during NBA0903B post-test autopsy. Right side rib fractures may have occurred during initial 3 m/s impact to subject's right hand side.

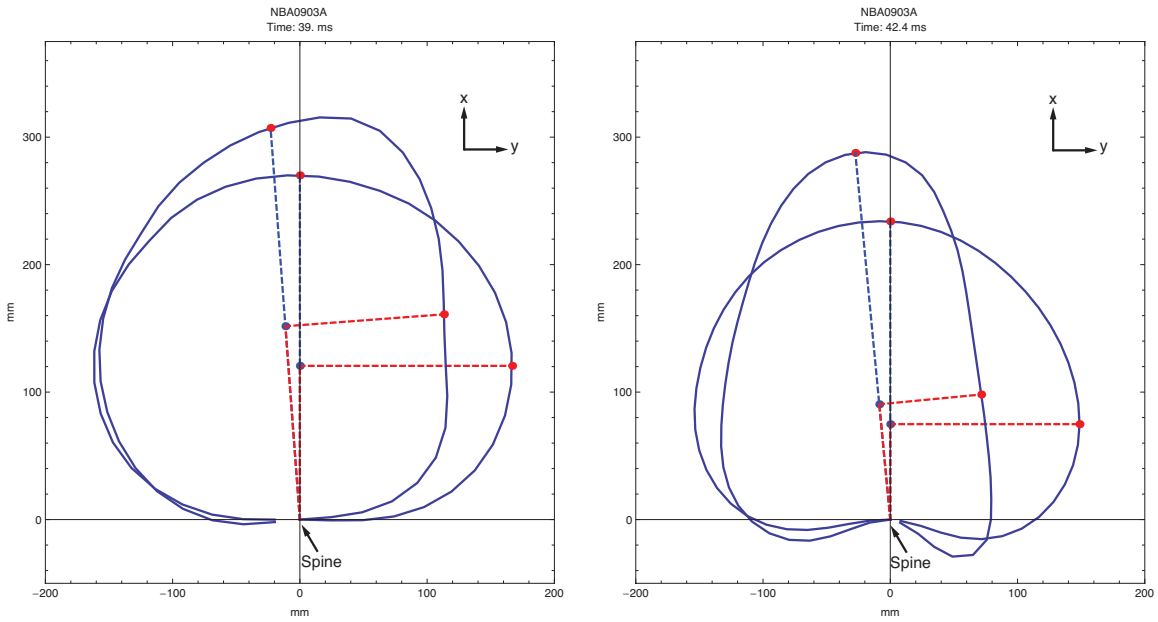

Figure B6. NBA0903A thorax (left) and abdomen (right) chestband contours.

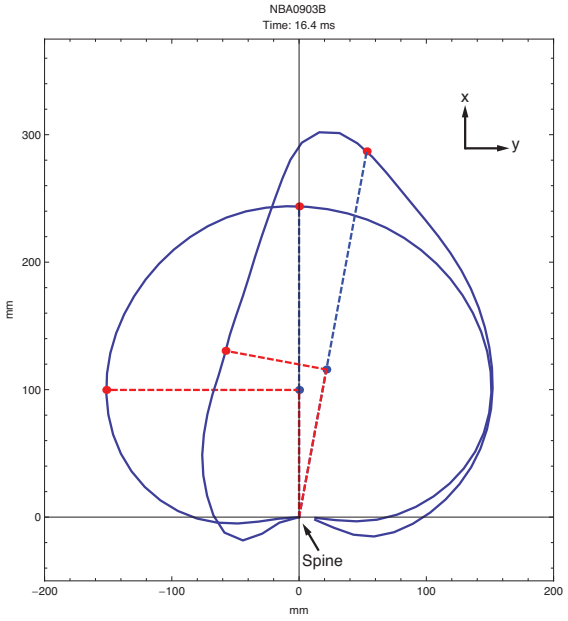

Figure B7. NBA0903B abdomen chestband contour.

NBA1004

Subject: Male, 66 years, 79 kg

NBA1004A: 3 m/s (initial impact, RHS)

Thorax deflection:	48 mm
Abdomen deflection:	88 mm
Injuries:	No injuries

NBA1004B: 8 m/s (second impact, LHS)

Thorax deflection:	46 mm
Abdomen deflection:	75 mm
Injuries:	No injuries

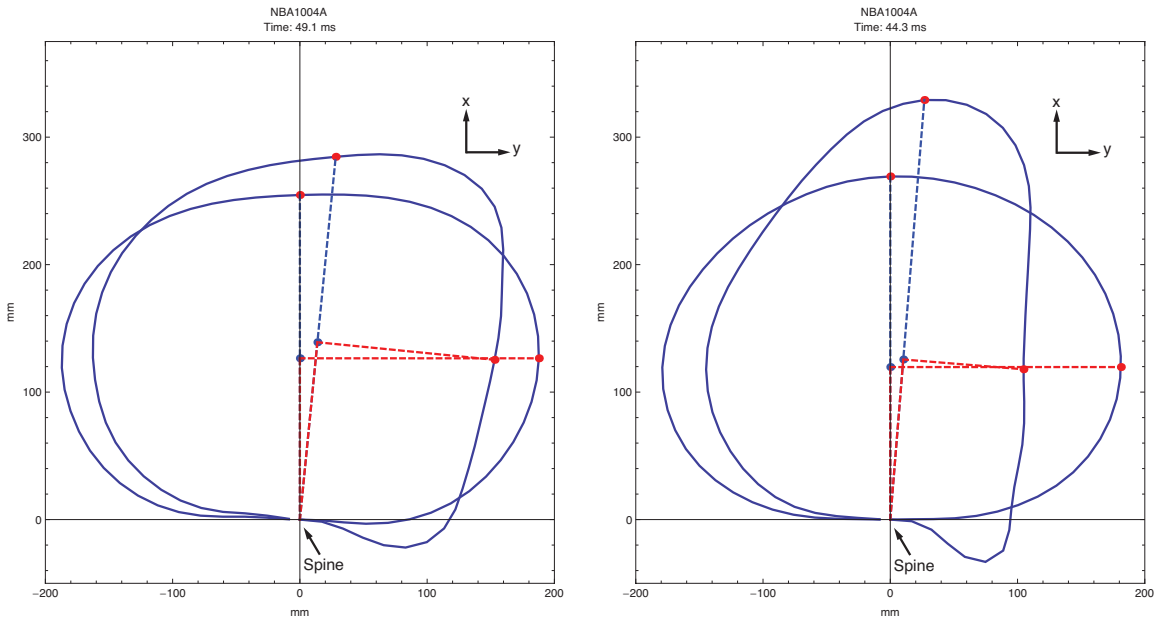

Figure B8. NBA1004A thorax (left) and abdomen (right) chestband contours.

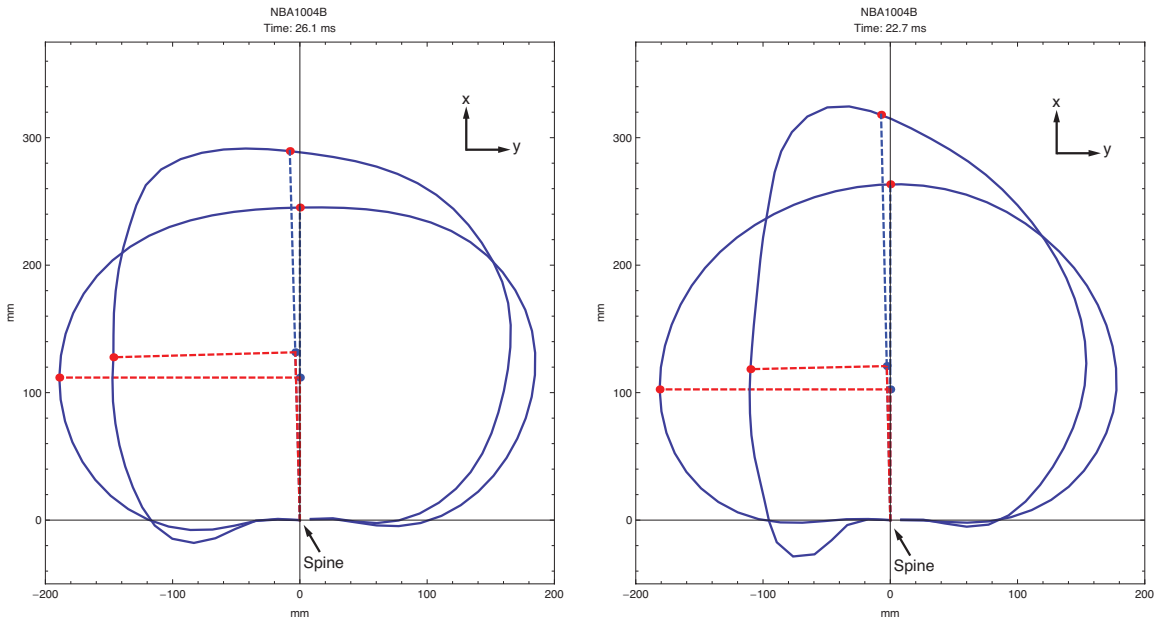

Figure B9. NBA1004B thorax (left) and abdomen (right) chestband contours.

NBA1005

Subject: Male, 51 years, 98 kg

NBA1005A: 3 m/s (initial impact, RHS)

Thorax deflection:	42 mm
Abdomen deflection:	79 mm
Injuries:	No injuries

NBA1005B: 8 m/s (second impact, LHS)

Thorax deflection:	66 mm
Abdomen deflection:	86 mm
Injuries:	Left 4th-6th anterior-lateral rib fxs, laxity in costo-sternal joints for left ribs 5 and 6

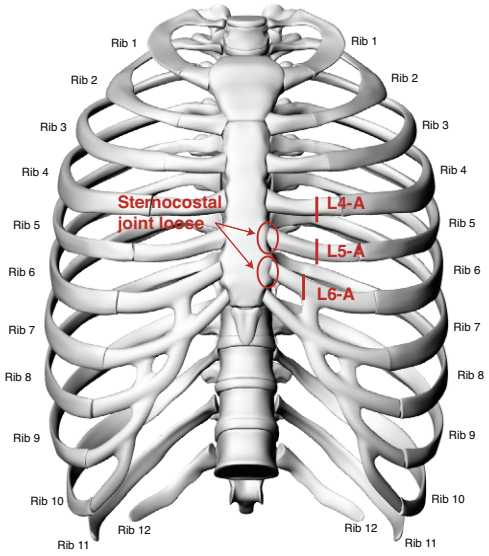

Figure B10. Locations of rib fractures as determined during NBA1005B post-test autopsy.

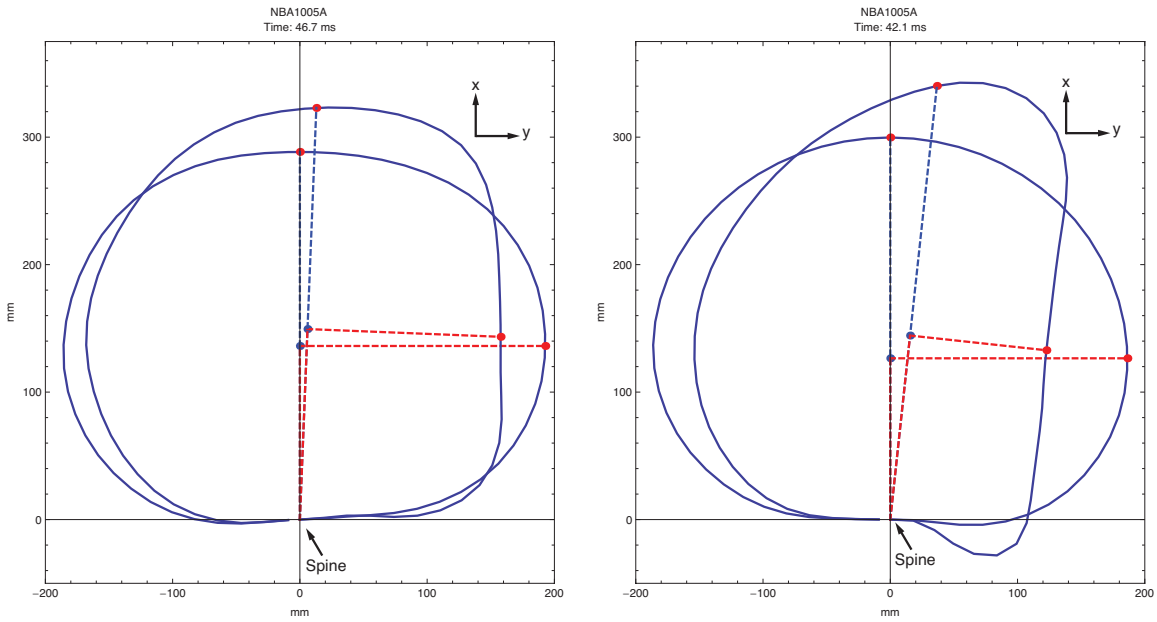

Figure B11. NBA1005A thorax (left) and abdomen (right) chestband contours.

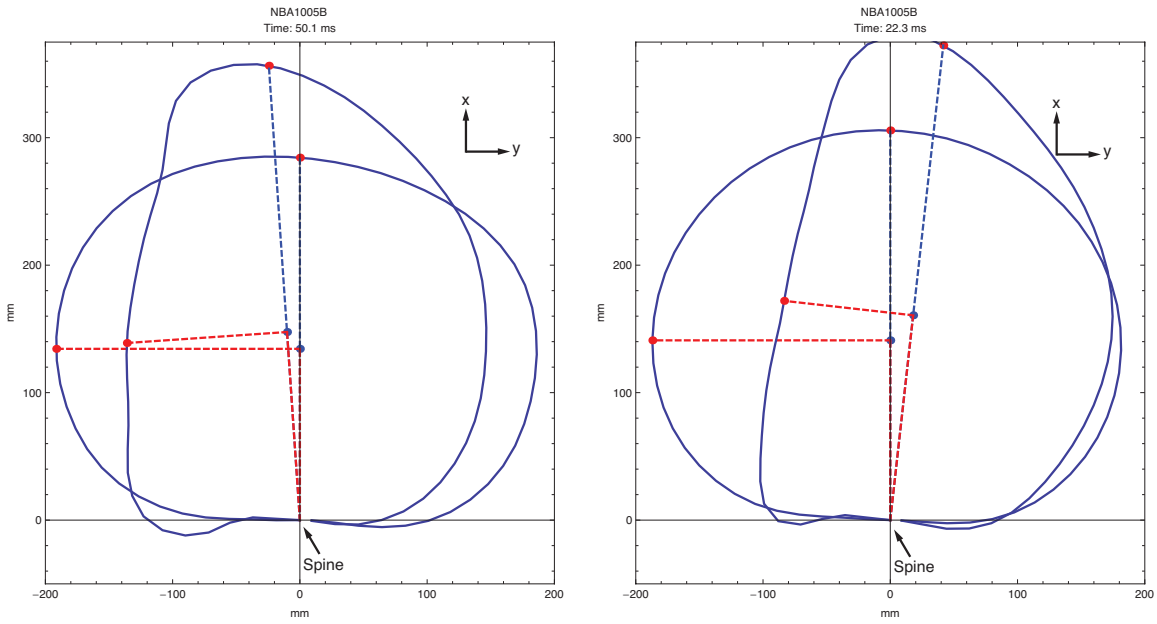

Figure B12. NBA1005B thorax (left) and abdomen (right) chestband contours.

NBA1006

Subject: Male, 34 years, 102 kg

NBA1006A: 3 m/s (initial impact, RHS)

Thorax deflection:	56 mm
Abdomen deflection:	80 mm
Injuries:	No injuries

NBA1006B: 8 m/s (second impact, LHS)

Thorax deflection:	59 mm
Abdomen deflection:	77 mm
Injuries:	Left lateral rib 5 fx

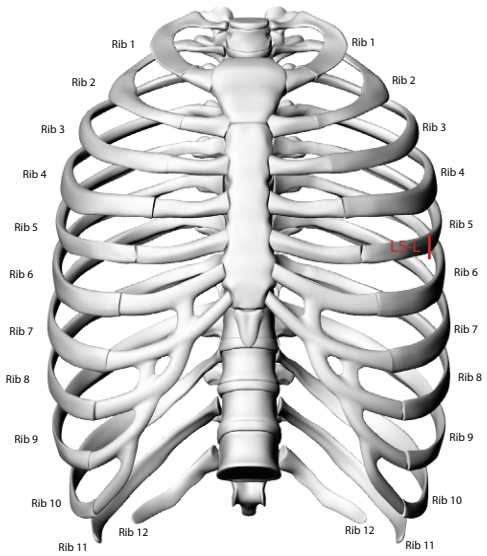

Figure B13. Location of rib fracture as determined during NBA1006B post-test autopsy.

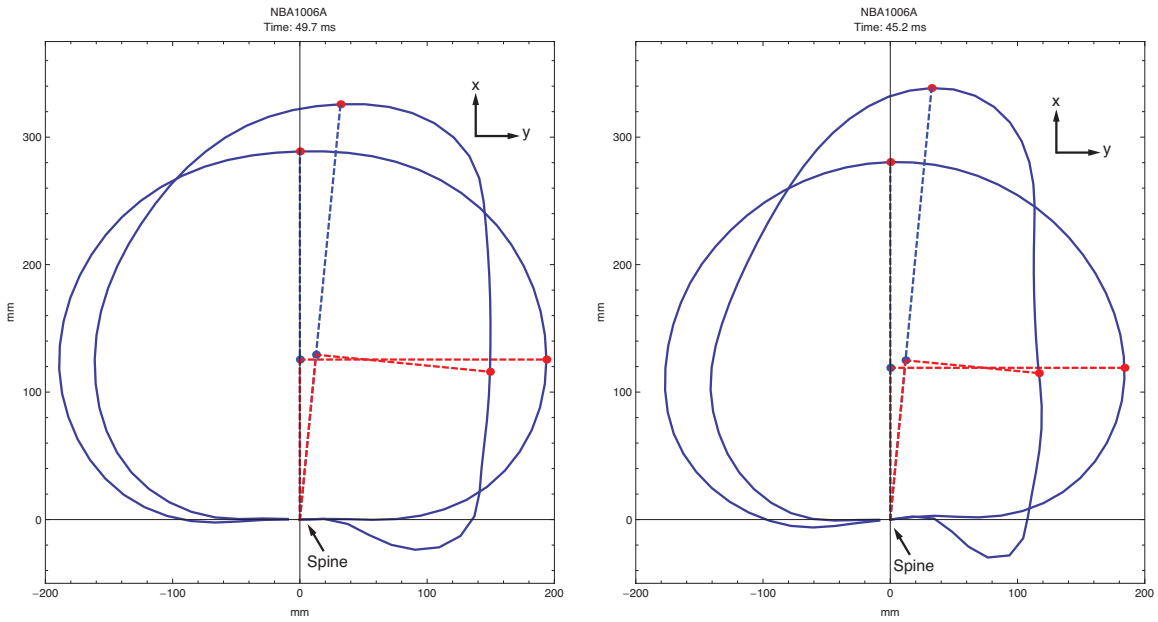

Figure B14. NBA1006A thorax (left) and abdomen (right) chestband contours.

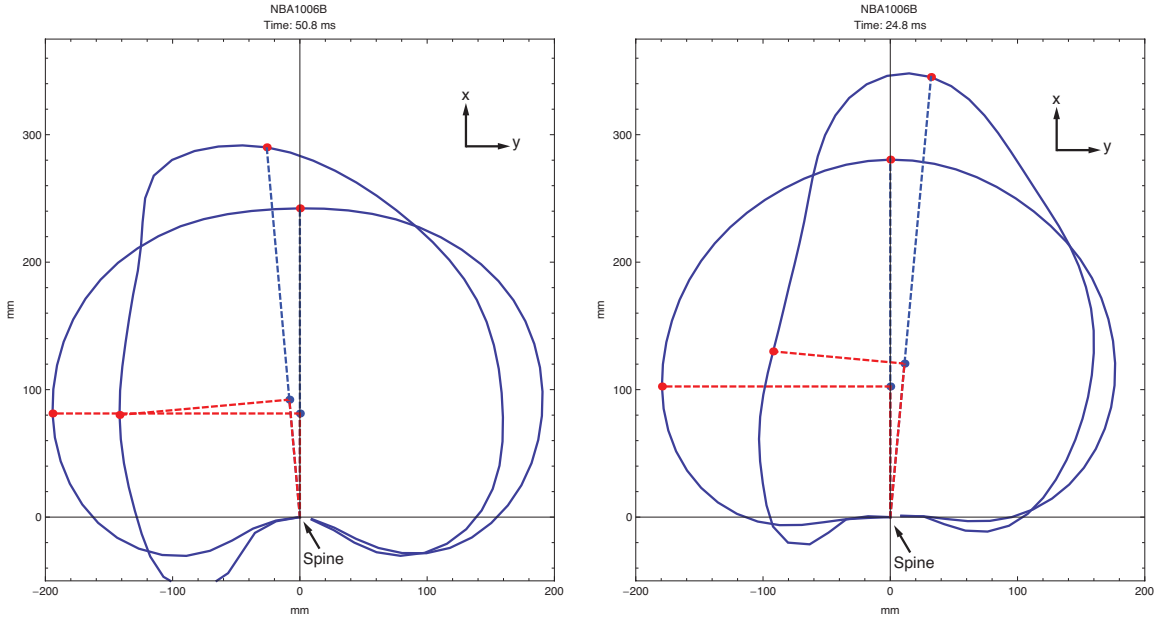

Figure B15. NBA1006B thorax (left) and abdomen (right) chestband contours.

NBA1007

Subject: Male, 87 years, 73 kg

NBA1007A: 3 m/s (initial impact, LHS)

Thorax deflection:	56 mm
Abdomen deflection:	79 mm
Injuries:	Left rib 7 lateral fx, and left rib 8 anterior-lateral and lateral fxs (preexisting right 7th rib anterior-lateral fracture)

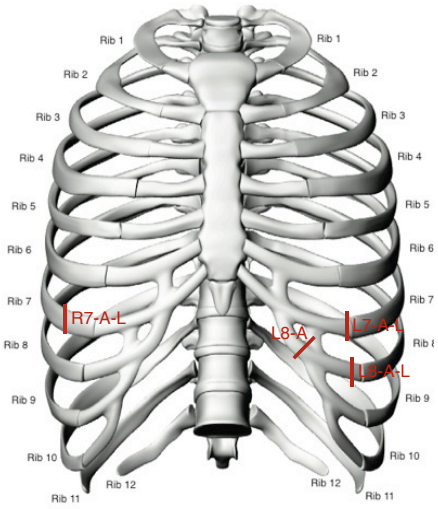

Figure B16. Locations of rib fractures as determined during NBA1007A post-test autopsy (shown right rib fracture was preexisting).

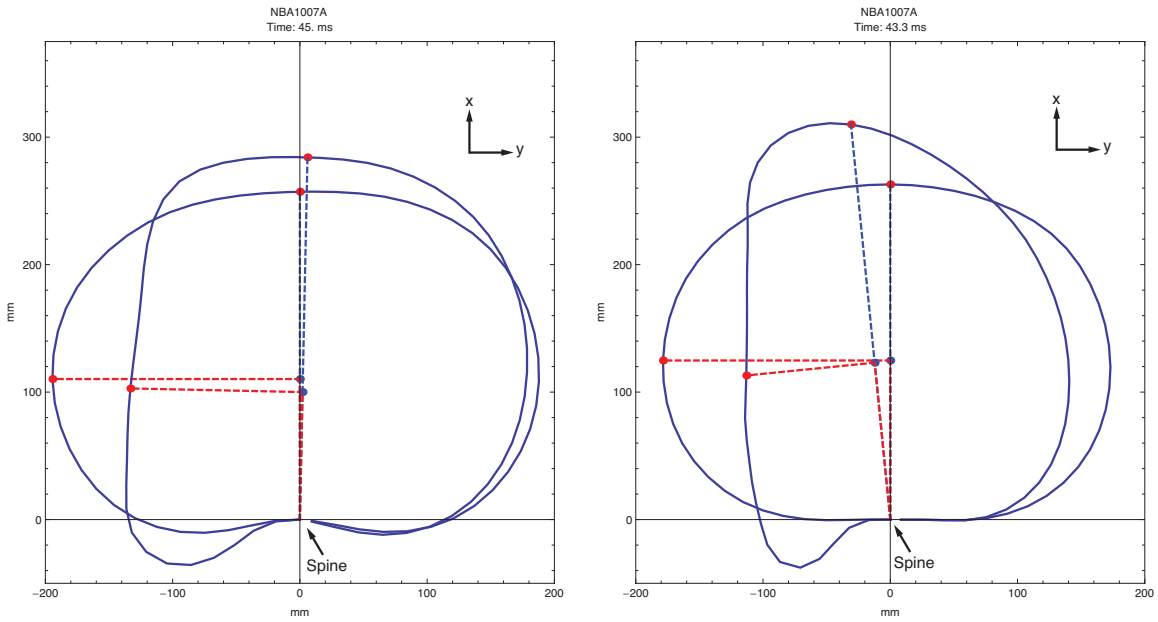

Figure B17. NBA1007A thorax (left) and abdomen (right) chestband contours.

APPENDIX C – SUBJECT RESPONSE CURVES

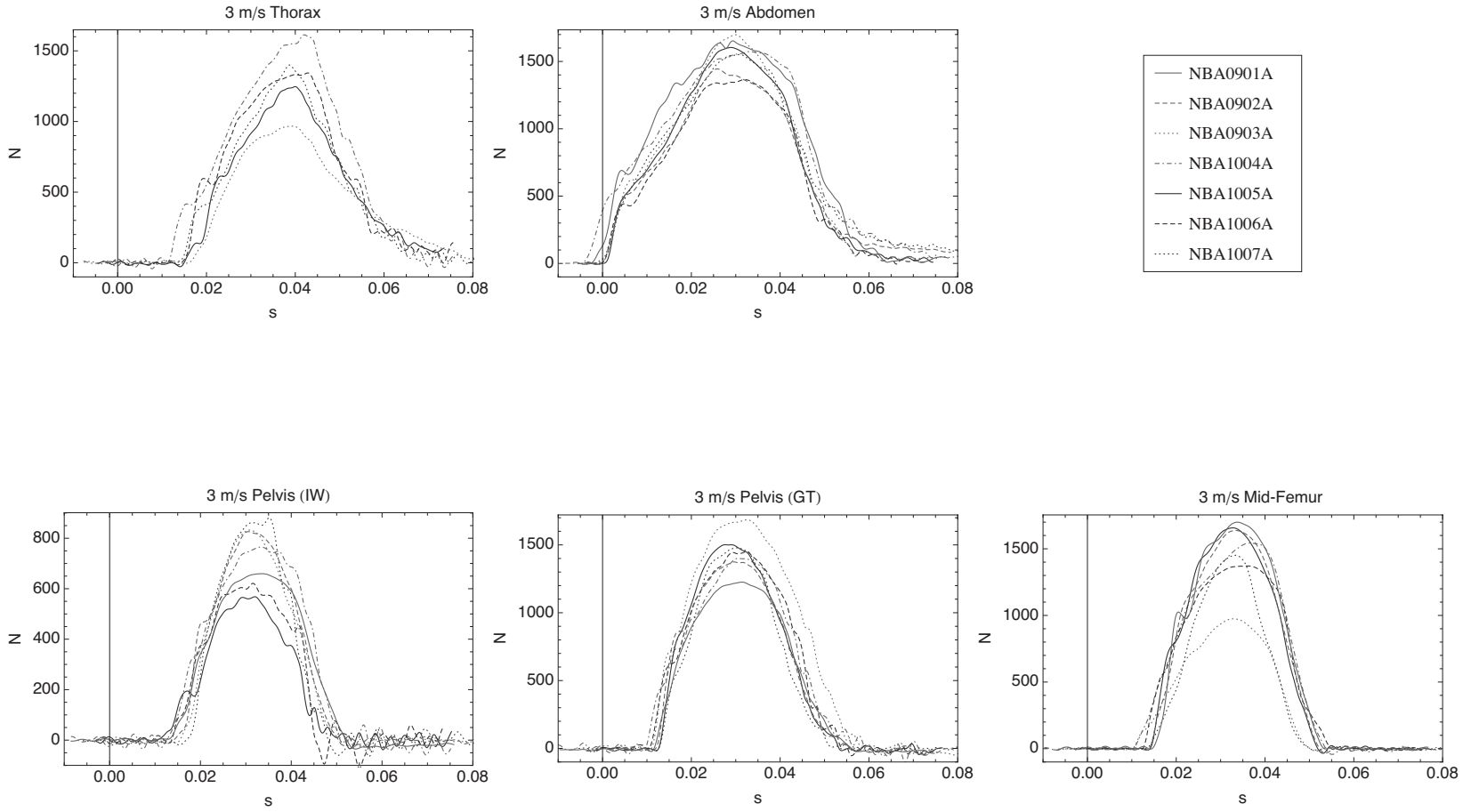

Figure C1 Scaled applied force histories for the thorax (top left), abdomen (top right), iliac wing (bottom left), greater trochanter (bottom middle), and mid-shaft femur (bottom right) for the 3-m/s tests.

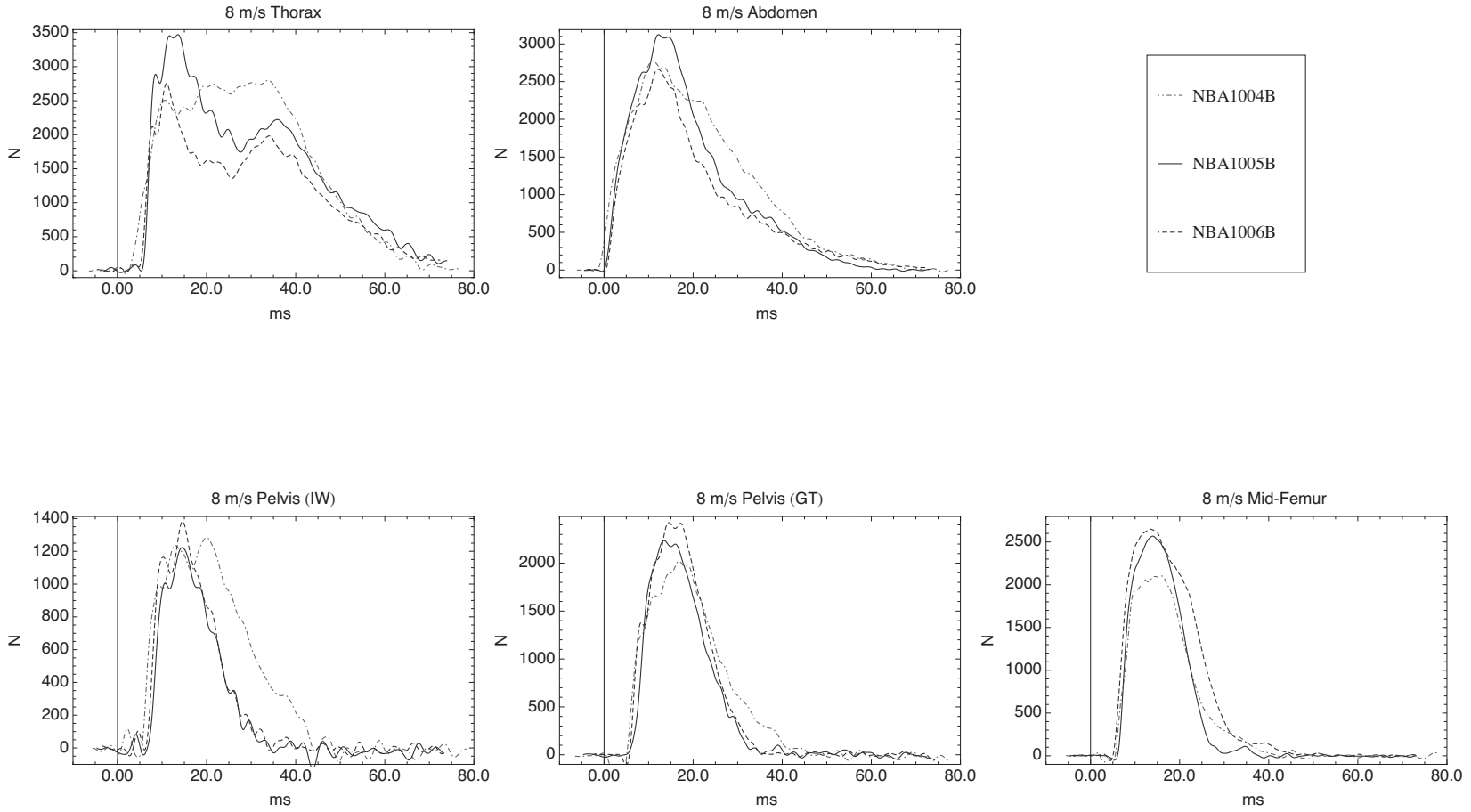

Figure C2. Scaled applied force histories for the thorax (top left), abdomen (top right), iliac wing (bottom left), greater trochanter (bottom middle), and mid-shaft femur (bottom right) for the 8-m/s tests.

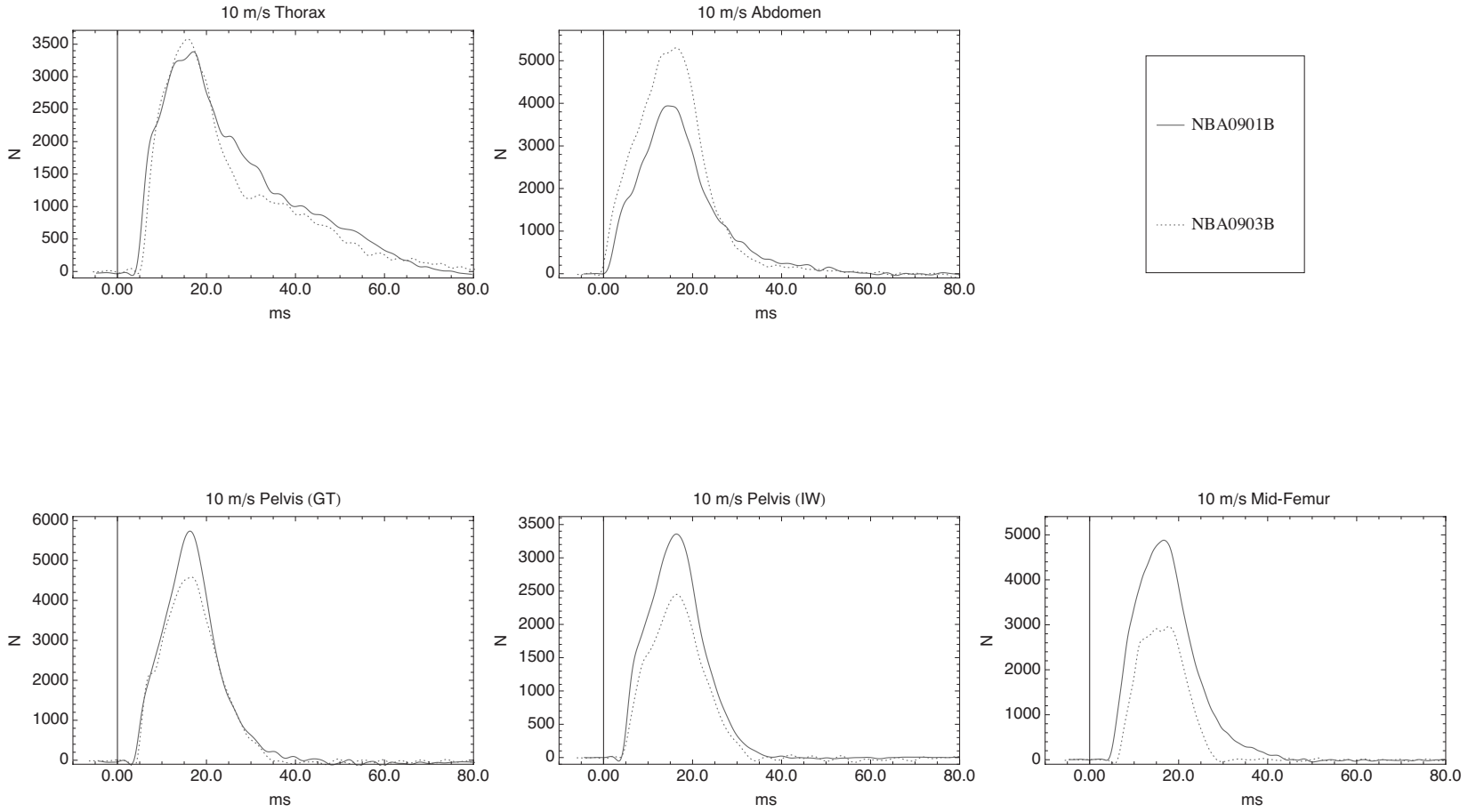

Figure C3. Scaled applied force histories for the thorax (top left), abdomen (top right), iliac wing (bottom left), greater trochanter (bottom middle), and mid-shaft femur (bottom right) for the 10-m/s tests.

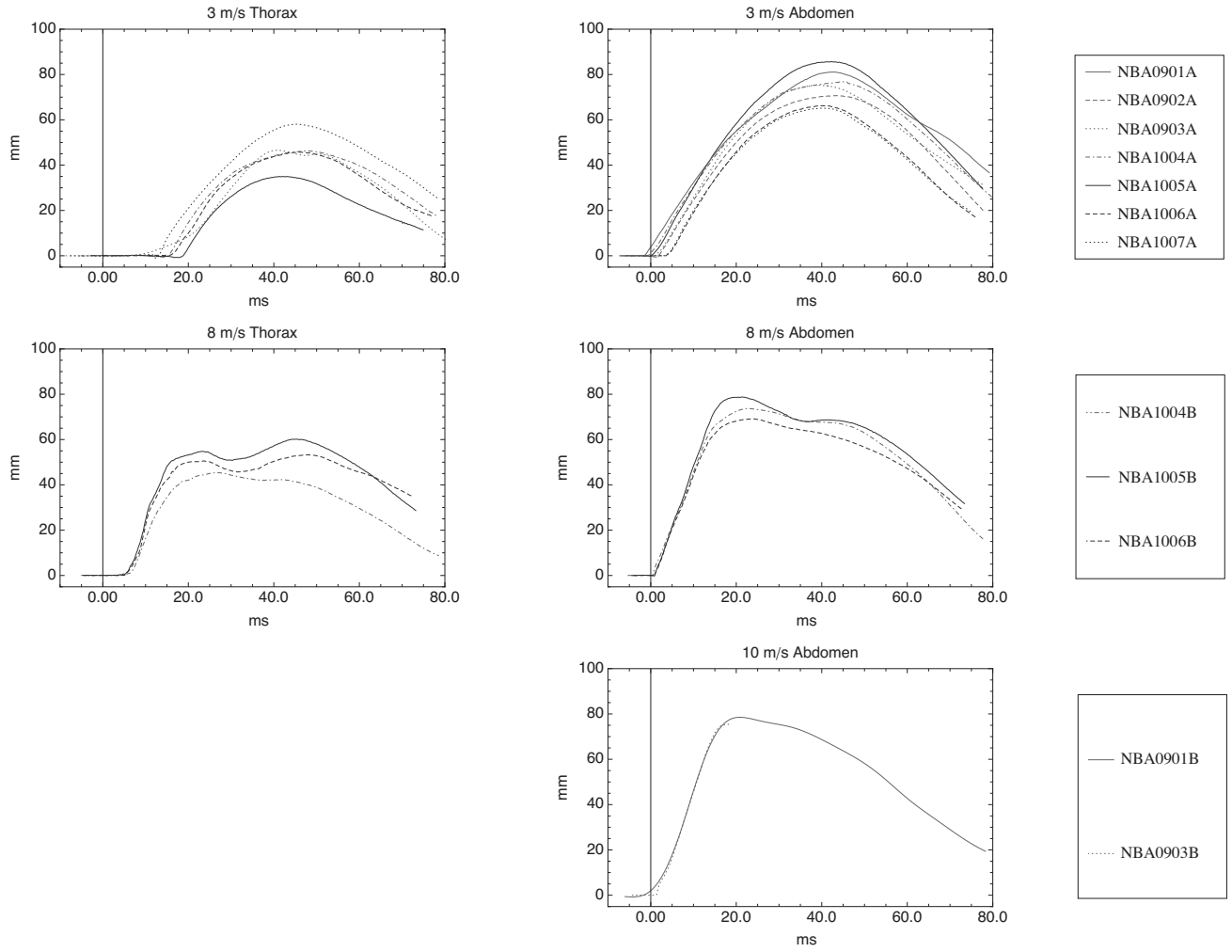

Figure C4. Scaled external thorax and abdomen deflection histories for 3- (top row) and 8-m/s (middle row) test conditions and scaled external abdomen deflection histories for the 10m/s (bottom row) test condition.